Graduation Thesis Report
on

Analysis of radio downlink in Social XR scenarios involving 5G channel state information acquisition techniques

Submitted by

Sandra Kizhakkekundil
Student ID-5050731
Technische Universiteit Delft

Under the guidance of

Dr. Remco Litjens M.Sc.
Associate Professor-TU Delft, Senior Scientist-TNO
Ir. Sjors Braam
Research Scientist-TNO

Thesis committee

Dr. Remco Litjens M.Sc.
TU Delft, TNO
Prof. Dr. Alexander Yarovoy
TU Delft

Department of Electrical Engineering Mathematics and Computer Science - TU Delft
Department of Networks - TNO

Department of Electrical Engineering Mathematics and Computer Science (EEMCS)

Technische Universiteit Delft-TU Delft

Certificate

TU Delft supervisor	Date
Dr. Remco Litjens M.Sc.	xx-xx-2022
External	Date
Prof. Dr. Alexander Yarovoy	xx-xx-2022

Abstract

The Fifth Generation (5G) of mobile networks exploit both sub-6 GHz and millimeter-wave (mmWave) spectrum. The sub-6 GHz spectrum comprises frequencies up to 6 GHz and provides large geographical coverage for radio signal in 5G. The mm-wave spectrum on the other hand, comprises higher frequencies ranging from 24 GHz -100 GHz and plays a major role in serving high data rates for the 5G technology. The evolution of 5G plays a pivotal role in the realisation of challenging applications like Social XR conferences, which requires the network to deal with heavy traffic while maintaining low end-to-end latencies. The right configuration of the radio access network becomes crucial for such applications.

The introduction of Massive Multiple Input Multiple Output (MIMO) technology in the radio network, concentrates the signal energy to the target user, which significantly improves the throughput and efficiency of the system. The quality and capacity of the radio channels also depend on the downlink Channel State Information (CSI). The CSI when obtained accurately at the Base Station (BS), plays a significant role in reaping the best benefits out of Multiple Input Multiple Output (MIMO) technology. This thesis explores (or assesses) the different options and configurations of CSI feedback using an indoor Social Extended Reality (XR) conference application scenario. The performance analysis of the radio downlink while using the latest 5G New Radio (NR) *Types I* and *II* CSI which use a DFT-based codebook are detailed. The impact of the codebook-related configurable parameter of Rotation Factor (RF), the performance variations while using a 'fixed-RF' for all the UEs compared to the more flexible 'adaptive-RF', different beamforming technologies (Single-User MIMO (SU-MIMO) and Multi-User MIMO (MU-MIMO)), transmission ranks and co-scheduling parameter values are assessed using the key performance metric of Packet Loss Ratio (PLR). The frequency bands of 3.5 GHz (sub-6 GHz spectrum) and 26 GHz (mmWave spectrum) are chosen for the thesis and performance variations between the two bands are studied. The key insight from the thesis research is that the 'adaptive-RF' case gives the optimal performance for the considered Social XR scenario when we set the right co-scheduling parameters (which balance the encountered interference and frequency of co-scheduling).

Keywords: Channel state information, *Type I* **CSI,** *Type II* **CSI, Social XR, interference estimation, MIMO, MU-MIMO, SU-MIMO, 5G, RAN, beamforming, grid of beams.**

Contents

Abbreviations

3GPP 3rd Generation Partnership Project

5G Fifth Generation

AE Antenna Element

AR Augmented Reality

AZ Azimuth

BLER BLock Error Rate

BS Base Station

CQI Channel Quality Indicator

CRI CSI-RS Resource Indicator

CSI Channel State Information

CSI-RS Channel State Information Reference Signal

DFT Discrete Fourier Transform

EL Elevation

FDD Frequency-Division Duplex

GoB Grid of Beams

GoP Group of Pictures

HMD Head-Mounted Display

HPBW Half Power Beam Width

L1-RSRP Layer 1 Reference Signal Received Power

LC Linear Combination

LI Layer Indicator

LOS Line of Sight

LTE Long Term Evolution

M-LWDF Modified-Largest Weighted Delay First

MCS Modulation and Coding Scheme

MIMO Multiple Input Multiple Output

MPM Multi-elliptical Propagation Model

MR Mixed Reality

MRC Maximum Ratio Combining

MU-MIMO Multi-User MIMO

NLOS Non Line of Sight

NR New Radio

PER Packet Error Rate

PLR Packet Loss Ratio

PMI Precoding Matrix Indicator

PSK Phase Shift Keying

PUSCH Physical Uplink Control Channel

PUSCH Physical Uplink Shared Channel

Quadriga QUAsi-DeteRministic RadIo channel GenerAtor

RF Rotation Factor

RI Rank Indicator

RTT Round Trip Time

SINR Signal-to-Interference-plus-Noise-Ratio

SRS Sounding Reference Signal

SSBRI SS/PBCH Resource Indicator

SU-MIMO Single-User MIMO

TDD Time-Division Duplex

TTI Transmission Time Interval

UDP User Datagram Protocol

UE User Equipment

ULA Uniform Linear Array

URA Uniform Rectangular Array

VR Virtual Reality

XR Extended Reality

Acknowledgments

I would like to thank TU Delft for providing me with the courses of my interest, which helped me hone my technical knowledge and for giving me an environment to further enhance my skills in specific areas of interest through my graduation thesis research.

I would like to thank TNO for providing me with the internship opportunity through which I could improve my knowledge and skills on a wide scale. Through the course of the thesis, I met and had fruitful interactions with a lot of intellectuals at the organisation.

I am extremely grateful to my supervisors Dr. Remco Litjens M.Sc. and Ir. Sjors Braam for their constant guidance and support. Their valuable comments helped to streamline and fine-tune my thoughts at every juncture of the thesis process.

I would like to extend my gratitude towards Prof. Dr. Alexander Yarovoy for participating in the the defence committee as the external panel member.

A special mention and thanks to my student mentor, João Morais for the continuous technical guidance and very valuable insights throughout the course of the project.

I am eternally grateful to have the constant support of my husband Dheeraj for all the emotional and moral boost and being all ears to my technical rambling.

Last but not the least, I would like to thank my Mom and Dad for being my pillars of strength.

Chapter 1

Introduction

With the demand for mobile data traffic increasing at an exponential rate, incorporation of massive MIMO technology plays a pivotal role in 5G New Radio (NR) systems. Massive MIMO systems consist of Base Stations (BSs) equipped with a large number of transmit antennas which concentrate the signal energy to a specific user instead of broadcasting the data throughout the coverage area. This results in significant improvement of signal strength. In addition, there is a potential increase in the number of users served simultaneously using the same time-frequency resources since multiple beams can be allocated to single or multiple users [27]. This incorporation majorly contributes to improving the spectral efficiency and network performance enabling 5G systems to achieve throughput in the range of gigabits per second.

The quality and capacity of the radio channels also depend on effective scheduling mechanisms that provide optimal bandwidth and coverage to each user while reducing inter-layer (layers refer to the data streams which are co-scheduled simultaneously and are directed either towards the same or different user) and inter-cell interference considerably. Such mechanisms rely heavily on the 5G base station to be fed with adequate downlink Channel State Information (CSI) obtained either through feedback from the user or derived from uplink Sounding Reference Signal (SRS), which helps in selecting the best beam for data traffic towards the user, resulting in highest attainable throughput.

A number of works in existing literature involve performance analysis comparison of radio downlink using different methods of obtaining CSI in Long Term Evolution (LTE) and 5G NR technologies. The optimal codebook design for these technologies, such as those based on Discrete Fourier Transform (DFT) and Grassmannian methods, is also a widely followed related research area. Recent works focus on reducing the CSI feedback overhead using data compression and machine learning techniques.

Both Time-Division Duplex (TDD) and Frequency-Division Duplex (FDD)-based CSI techniques include some configurable parameters, which significantly affect the downlink performance. However, there is not much work focusing on this part of the research. Through this thesis, 3rd Generation Partnership Project (3GPP) recommended state-of-the-art CSI mechanisms are analysed in the context of a simulated Social XR indoor conference scenario. The first configurable parameter for the codebook, which can significantly affect the system performance is identified as the Rotation Factor (RF), which comprises of a set of mutually orthogonal precoders for the UEs (the details are presented in Chapter 2 and 3). The literature does not specify whether the RF is fixed to a specific

value for all UEs (we refer to this setting as 'fixed-RF' from now on), or if the UEs individually get to pick the best RF suitable for them (we refer to this setting as 'adaptive-RF' from now on). Since this 'fixed/adaptive-RF' is not standardised, it is relevant to compare the options. The trade-off involved for the benefits of having more tailored beams in the 'adaptive-RF' include either higher or the same overhead as the 'fixed-RF' case. This overhead can be compensated by the less frequent and consequently less up-to-date CSI feedback for the 'adaptive-RF' case compared to its counterpart.

The thesis investigates the performance analysis of downlink radio channel for the conference scenario for both 2.5 GHz and 26 GHz frequency bands using different MIMO technologies (SU-MIMO and MU-MIMO) with different transmission ranks, where 3GPP recommended $Type\ I$ and $Type\ II$ CSI feedback mechanisms are deployed with 'fixed-RF' and 'adaptive-RF' cases. Another important configurable parameter called the co-scheduling parameter (γ) is introduced and the impact analysis of the same is performed in combination with the aforementioned methodologies. For the optimal performance configurations obtained from amongst the different cases, the thesis also includes a bandwidth analysis for both frequency bands, to understand the minimum bandwidth values suitable to attain the target Packet Loss Ratio (PLR) performance.

The rest of the report is organised as follows. Chapter 2 starts with the background and literature study related to the significance of CSI and the classification of methodologies used to obtain the same. The design and details of the DFT-based codebooks used for $Type\ I$ and $Type\ II$ CSI methods as standardised by 3GPP, are covered. This is followed by a brief definition of Social XR application with examples and basic requirements for a typical application cited from literature. The chapter concludes with a statement of the key contributions of this thesis.

Chapter 3 describes the key modelling aspects underlying the presented performance study. This includes a specification of the Social XR use case scenario, the application characteristics and requirements covering the Base Station (BS) antenna configurations and the user behavior, the network deployment and the radio resource management covering the $Type\ I$ and II CSI modelled codebook characteristics, scheduling mechanisms and the beam-based book-keeping interference estimation for $single$ and $dual-rank$ cases for Single-User MIMO (SU-MIMO) and Multi-User MIMO (MU-MIMO).

Chapter 4 presents the results and detailed analysis of the modelled application scenarios using the PLR metric and investigates how the performance of the Social XR use case described in Chapter 3 varies with different frequency bands, CSI feedback techniques, RFs, MIMO techniques, transmission ranks and co-scheduling parameter values using the Social XR simulator.

Chapter 5 summarizes and concludes the thesis work by presenting the key results and observations along with suggestions for potential future work.

Chapter 2

Background and literature study

The purpose of this chapter is to explain the core concepts of the thesis and also provide an overview of the most relevant literature. Since the crux of the thesis is the assessment of comparison of different options and configuration for CSI acquisition techniques in a Social XR scenario, it is imperative that we explain the significance of the technology and the application we base our thesis upon. The first section explains the relevance of CSI in 5G radio access networks along with the different methods of obtaining it. The second section covers the background study about Social XR applications. The final section details the contributions of the thesis.

2.1 Beamforming and MIMO

Beamforming is a signal processing technique which involves tuning the amplitude and phase of the signal fed to each antenna element of an antenna array to create constructive interference at a particular point in space, thus improving the signal transmission or reception at that point. The signals from each antenna can also be made to destructively interfere by using the same approach to reduce the interference affecting other transmissions. At higher frequencies like mm-wave, the increase in antenna gain/coverage produced by beamforming is used to overcome the severe signal attenuation.

MIMO is an antenna technology which makes use of multiple antennas both at the BS and the UE. These antennas are combined to optimize the data speed, minimize errors and enhance the radio transmission capacity by allowing data to traverse multiple signal paths in parallel. Traditional MIMO technology provides increased link coverage and data throughput in wireless communications without a corresponding increase in transmit power or serving bandwidth. MIMO can also enhance spectral efficiency and hence cell capacity. MIMO comes in two flavours: SU-MIMO and MU-MIMO. In SU-MIMO, the BS sends one or more data streams to a single User Equipment (UE) using the same time-frequency resources. In MU-MIMO, the BS transmits multiple data streams directed towards multiple users using the same resources. The maximum benefit of MIMO technology with respect to the attainable performance relies on the CSI feedback accuracy at the transmitter.

2.2 Channel state information

The signal which propagates from the BS to the UE gets affected by factors like fading, distance-dependent power decay and scattering. The downlink CSI reflects this informa-

tion. The UE extracts this information from the reference signals sent by the BS also known as Channel State Information Reference Signal (CSI-RS). The UE then generates a CSI report which is fed back to the BS. The BS on possession of this CSI report, can maneuver or precode the beam directed towards the UE in such a way that it best tunes the transmission parameters (E.g. determine the most suitable beam, perform scheduling, Modulation and Coding Scheme (MCS) selection) in line with the aforementioned factors. Precoding is a well known technique where the data is precoded prior to transmission based on the channel knowledge. Each antenna's transmit signal is coded with different amplitude and phase to spatially direct the signal.

The downlink CSI acquisition methods can be broadly categorised into codebook-based and SRS-based (codebook-free) approaches. While TDD systems support both the approaches, FDD systems only support the codebook-based method. The white papers [36] and [41] indicate that the current mobile operators prefer to use a combination of both SRS-based and codebook-based methods, in the sense that SRS-based CSI acquisition is followed when there is good coverage for the user, while for cell-edge users, the codebook-based acquisition method is followed. While the SRS-based approach can look like a potential candidate for a small-cell scenario, there are multiple factors which give an edge to the codebook-based approach. Compared to the SRS-based approach, the codebook-based approach can be configured simultaneously to serve much more users, since there is a limitation to the available SRS resources in a cell [36]. SRS-based approach also requires heavy system calibration (discussed in Section 2.2.1). Also, the codebook-based approach is the common method covered in both TDD and FDD systems. Hence, the thesis focuses on the codebook-based approach.

CSI reporting

Though the thesis considers only downlink CSI analysis, it is worthwhile to understand the high level contents of the CSI report which is fed back to the BS in the uplink, which enables the BS with the channel knowledge. In Fifth Generation (5G) NR, the contents of the CSI report obey the following structure [1]:

- **reportConfigType**: This parameter specifies the scheduling periodicity of the report and the channel used for sending the report to the BS. The reports can be sent periodically using the Physical Uplink Control Channel (PUSCH), a-periodically using the Physical Uplink Shared Channel (PUSCH) or in a semi-persistent manner using either the PUCCH or the PUSCH.

- **reportQuantity**: This parameter specifies the report measurement type. The two type of quantities which can be measured are CSI-related and Layer 1 Reference Signal Received Power (L1-RSRP)-related. The thesis focuses on the CSI-related report quantities which depend on the type of CSI acquisition method and are detailed in the upcoming subsections.

- **reportFreqConfiguration**: This parameter specifies the granularity of the report in frequency domain. The reporting can be performed on wideband or subband basis.

- **timeRestrictionForChannelMeasurements** : This parameter if configured, enables time domain restrictions for channel measurements.

- **timeRestrictionForInterferenceMeasurements** : This parameter if configured, enables time domain restrictions for interference measurements.
- **codebookConfig** : The codebook-based downlink CSI acquisition requires the configuration of number of parameters, which are reported through the codebookConfig. The exact parameters and their values are detailed in the upcoming subsections.

.

2.2.1 SRS-based CSI acquisition

In TDD systems the downlink and uplink share the same frequency carrier. Due to this, the concept of channel reciprocity [17] can be exploited here to estimate the downlink channels and this is a very common method followed in many studies and models of massive MIMO [19, 20, 35]. In ideal cases when TDD systems achieve perfect channel reciprocity, the uplink and downlink transmission links match exactly. Hence, the SRS transmitted by the UE in the uplink can be used for determining the precoding weights of the downlink.

The reportQuantity of the CSI report in this case predominantly consists of the Channel Quality Indicator (CQI), Rank Indicator (RI), and Layer Indicator (LI). CQI indicates the downlink channel quality (detailed values can be referred with table 5.2.2.1-2 in 3GPP TS 38.214 [1]), RI indicates the downlink transmission rank and LI indicates the strongest layer amongst the set of layers reported by RI.

The communication channel also consists of elements like antennas, filters, RF mixers and A/D converters which may not be identical for all devices. Hence the major shortcoming of this method lies in the calibration requirement of the system before the exploitation of reciprocity.

2.2.2 Codebook-based CSI acquisition

In FDD systems the downlink and the uplink use distinct frequency carriers making the downlink channel derivation from channel reciprocity impossible. Codebook-based CSI mechanism happens when the UE feeds back the CSI to the BS in order to help optimize the downlink MIMO precoding, scheduling and MCS selection. The feedback is based on a 3GPP-standardised codebook consisting of a set of precoders. Precoders are a set of beamforming weights which when applied to the BS antennas help steer them in a desired direction, in this case in the direction of the strongest path towards the UE. In TDD systems, the codebook-based CSI acquisition in considered in case the SRS may not be received strong enough (cell edge users) and also in general, considering the shortcomings of the SRS-based approach detailed in the Section 2.2. This CSI acquisition method supports both TDD and FDD systems and can be of two types, namely *Type I* and *Type II* CSI feedbacks. These are standardized by 3GPP as *Type I* codebook (3GPP LTE and NR) and *Type II* codebook (3GPP NR). Both codebook types are 2D DFT-based codebooks covering the beamforming in both azimuth and elevation planes (also called full-dimension beamforming).

The reportQuantity in the CSI report in this case consists of the CQI, RI, LI and Precoding Matrix Indicator (PMI). The PMI is a pointer to the index of the best precoder or codeword in the table of all possible precoders maintained at both UE and BS ends.

Codebook design for an optimal CSI feedback is a research field in itself. The Grassmannian line-packing codebook proposed in [25] assists the beamforming aided systems communicating over spatially independent channels. Another Grassmannian based codebook called the Grassmannian subspace packing codebook proposed in [24] caters spatial multiplexing assisted systems. Spatially correlated channels are explored through a modified Grassmannian-based codebook is proposed in [34]. DFT-based codebooks are simple structured codebooks which are easier to create, and produce uniformly spaced weights in the specified spatial domain. In systems deploying traditional MIMO technology, DFT-based codebooks are preferred over others considering their effectiveness in precoding antennas for spatially correlated channels [23, 38, 39, 40]. [40] also presents a comparative study between DFT-based and Grassmannian-based codebooks and proves the effectiveness of the former for spatially correlated channels. To summarise, DFT codebooks are more simple structured and scale-able compared to the Grassmannian codebooks. They also outperform the Grassmannian codebooks in case of high antenna correlation scenarios. However, for spatially uncorrelated channels or cases where UE has access to correlation information, Grassmannian codebooks have shown better performance compared to its counterpart.

DFT-based codebook

For a Uniform Rectangular Array (URA) type BS with single polarised Antenna Element (AE)s, a 2D DFT codebook (denoted by $W_{\text{single pol}}$) is required, which is created using a Kronecker product of Uniform Linear Array (ULA) codebooks in horizontal and vertical directions ($X_1 \otimes X_2$) and is given by Equation (2.1) [1]. Each column of the codebook thus created is a precoding vector and the column vectors can be thought of as a Grid of Beams (GoB), spanning all directions. X_1 (dimension $[N_1 \times N_1O_1]$) and X_2 (dimension $[N_2 \times N_2O_2]$), obtained through Equations (2.2 and 2.3) and illustrated in Figure 2.1, represent 1D DFT codebooks comprising of precoders for BS with horizontally and vertically aligned ULA respectively. The URA codebook $W_{\text{single pol}}$ is of dimension $[N_1N_2 \times N_1O_1N_2O_2]$. N_1 and N_2 are the number of BS antennas (subarrays) in horizontal and vertical directions respectively. O_1 and O_2 are the DFT oversampling factors in horizontal and vertical directions and effectively create additional grids of orthogonal precoders, with the notion that the grids are not orthogonal with respect to one another. The Figure 2.1 depicts the URA codebook for the oversampling choice of $O_1 = O_2 = 4$ and an assumed antenna array of 4 x 4 antennas (subarrays), where each circle in the figure corresponds a precoder. There are 16 orthogonal grids (beams grouped under 16 RF). The beams within each grid/group/RF are orthogonal to each other, but beams in one group need not necessarily be orthogonal to beams of other group (e.g. the color-coded red and blue sets are not orthogonal to each other.). If the oversampling factors are set to unity, there will only be a single RF grid present with a total of 16 precoders.

$$W_{single\ pol} = \left[X_1 \otimes X_2\right] \tag{2.1}$$

$$X_{1\ l=0,\ldots,N_1O_1-1} = \left[1 \quad e^{\frac{j2\pi l}{N_1O_1}} \quad \ldots \quad e^{\frac{j2\pi(N_1-1)l}{N_1O_1}}\right] \tag{2.2}$$

$$X_{2\ m=0,\ldots,N_2O_2-1} = \left[1 \quad e^{\frac{j2\pi m}{N_2O_2}} \quad \ldots \quad e^{\frac{j2\pi(N_2-1)m}{N_2O_2}}\right] \tag{2.3}$$

Since release 10, the 3GPP specifications for CSI codebooks which support dual polarized BS antennas and MIMO transmissions are often configured as a combination of two matrices as shown in Equation (2.4), where W_1 is a block diagonal matrix (dimension

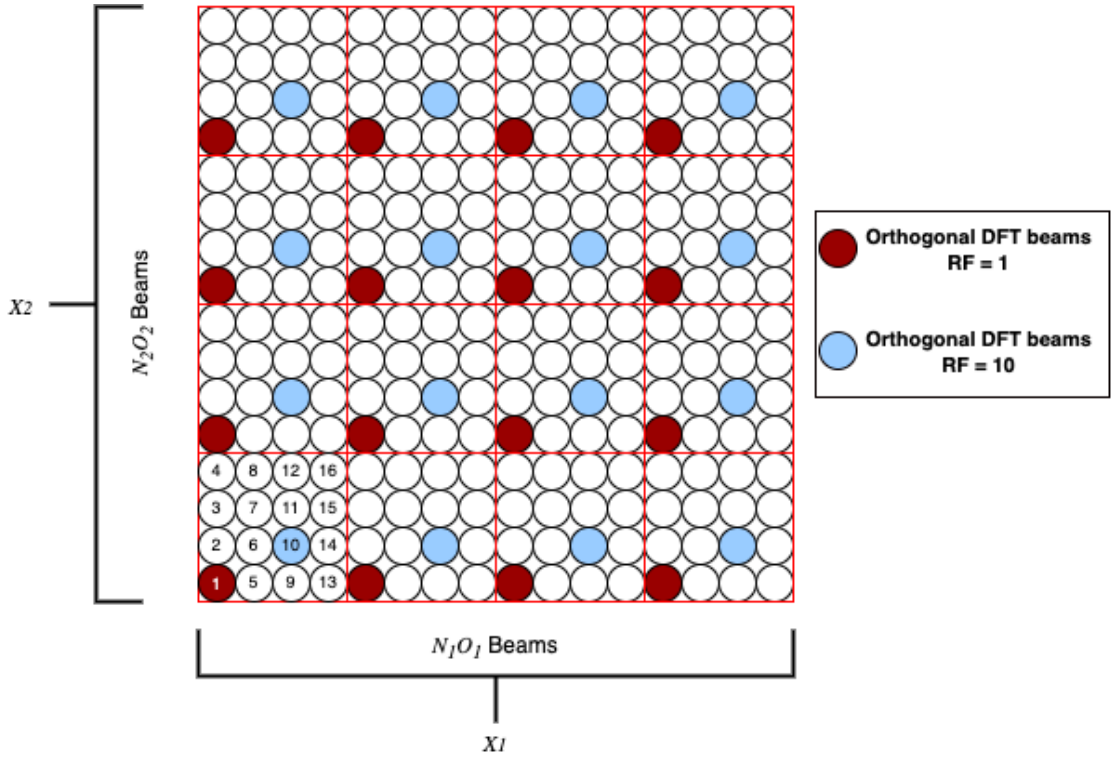

Figure 2.1: 2D DFT-based codebook structure for CSI for the oversampling choice of $O_1 = O_2 = 4$ and an assumed antenna array of 4 x 4 antennas (subarrays).

$[2N_1N_2 \times 2N_1N_2O_1O_2]$) as shown in Equation (2.5) and W_2 (dimension $[2N_1N_2O_1O_2 \times N_1N_2O_1O_2]$) is obtained through Equation (2.6). The codebook $W_{\text{dual pol}}$ is of dimension $[2N_1N_2 \times N_1N_2O_1O_2]$. The different column vectors of the matrix $[X_1 \otimes X_2]$ corresponds to different beam directions and the purpose of W_2 is to select the beamforming vectors from W_1 for each polarisation and co-phase or adjust the phase between the polarisations. Co-phasing is performed to obtain high gain from antennas and is performed by placing identical antennas at half-wavelength distance (dual polarised antenna array) and feeding them in-phase, to obtain 3 dB higher gain compared to a single polarised antenna array.

$$W_{dual\ pol} = W_1 \cdot W_2 \tag{2.4}$$

$$W_1 = \begin{bmatrix} X_1 \otimes X_2 & 0 \\ 0 & X_1 \otimes X_2 \end{bmatrix} \tag{2.5}$$

$$W_2 = \begin{bmatrix} 1 \\ e^{j\phi_1} \end{bmatrix} \tag{2.6}$$

$$W_{dual\ pol} = W_1 \cdot W_2 = \begin{bmatrix} X_1 \otimes X_2 & 0 \\ 0 & X_1 \otimes X_2 \end{bmatrix} \begin{bmatrix} 1 \\ e^{j\phi_1} \end{bmatrix} = \begin{bmatrix} X_1 \otimes X_2 \\ e^{j\phi_1} X_1 \otimes X_2 \end{bmatrix} \tag{2.7}$$

For single and dual rank transmissions per UE with a dual polarised URA type BS used in the thesis, the codebook is calculated using Equation (2.7). The co-phasing factor used for combining the beams selected from different polarisations is given by $e^{j\phi_1}$. This factor ϕ_1 can be a value from the set $[\pi/2, \pi, 3\pi/2, 2\pi]$ [1]. The total number of precoders in a codebook (columns in $W_{\text{dual pol}}$) is given by $N_1N_2O_1O_2$. The length of the precoding

vector (number of rows in $W_{\text{dual pol}}$) for a BS with dual polarised AEs ($2N_1N_2$) will be double that of single polarised AEs (N_1N_2).

The values of O_1 and O_2 depend on N_1 and N_2 and are standardised by 3GPP [1]. The detailed values are given in the modelling chapter. When the oversampling factors O_1 and O_2 are set to unity, precoding vectors in the resultant codebook are mutually orthogonal (e.g. in Figure 2.1, the red (or blue) color-coded precoders are mutually orthogonal). From an oversampled codebook ($O_1 > 1$ and/or $O_2 > 1$) of $W_{\text{single pol}}$ or $W_{\text{dual pol}}$, a column subset is selected by the BS such that all beamforming vectors are orthogonal. These subsets are represented by a RF and can have values ranging from 1 ... O_1O_2, each referring to a different subset of mutually orthogonal precoders (e.g. in Figure 2.1, the red color-coded precoders represent one RF and the blue color-coded precoders represent another subset of orthogonal vectors and hence a different RF). The values set for all the aforementioned codebook parameters are detailed in the modelling chapter.

The RF factor is a configurable parameter of the CSI codebooks, which play a vital role in the system performance and should be chosen wisely such that they give optimal results for the considered application environment. The existing literature does not provide much insight into any standard methodologies for fixing these values.

The BS can also optimise the downlink throughput by increasing the number of layers (also known as rank) of transmission, since this leads to a spatial multiplexing gain thereby contributing to throughput increase. The trade-off is the total transmit power of the system which gets reduced to $1/rank$ per layer and the possible inter-layer interference.

Type I CSI feedback

In *Type I* CSI based systems, the CSI report generated by the UE post reception of the CSI-RS signals from the BS, contains the PMI pointing at the single best precoder index from the DFT codebook, and is transmitted back to the BS through a feedback channel. This feedback mechanism approach is used in LTE and NR technologies [12]. The uplink overhead in this case is substantially low compared to the *Type II* CSI and the performance is observed to be satisfactory for SU-MIMO cases. For antennas with 4 or more CSI-RS ports [1], *Type I* codebook supports up to eight transmission layers (rank 8). The thesis considers single panel antennas and up to dual rank transmissions per UE mainly for two reasons: firstly for the sake of simplicity in analysis and secondly, for a fair comparison study since *Type II* CSI supports only up to dual rank transmissions per UE.

Type II CSI feedback

Type II mechanism is also known as the advanced or enhanced CSI feedback and includes more detailed and hence more accurate feedback from the UE to the BS at the cost of increased uplink overhead [6]. As mentioned before, both *Type I* and II CSI use the same DFT codebooks as a base for constructing the final precoder. While in *Type I* CSI, the UE chooses the best precoder directly from the base DFT codebook and feeds this back to the BS through a PMI, *Type II* performs a weighted linear combination of a selected group of precoders from the same codebook. The trade-off for the overhead of *Type II* lies in better CSI resolution to the BS, helping the BS to determine more suitable

[1] Total number of CSI-RS ports in a dual polarised antenna array equals the total number of antenna elements in the array.

precoders for serving the UE and effectively reduce inter-layer and inter-user interference of co-scheduled UEs and thus improve user- and/or cell-level performance. The additional directions to the strongest DFT beam direction could be relevant for estimating interference to potentially co-scheduled users and consequently influence both beamforming and co-scheduling decisions [12]. These additional beam information contributes to better CSI resolution and aids in MU-MIMO technology. Hence, the *Type II* was introduced mainly for serving the same. There are several studies attempting to reap the benefits of *Type II* CSI while reducing the uplink overhead through various data compression methods [18, 22, 28, 31]. While [28] uses reduced quantisation levels in feedback, [18, 22, 31] explore compressed sensing, neural networking and deep learning based intelligent feedback approaches.

Type II creates an Linear Combination (LC) precoder by using a linear combination of up to four best beams selected by the UE (denoted by parameter L with possible values of 2, 3 and 4) based on the CSI-RS signals. The value of L is configurable as per optimal performance of the system. A higher L implies higher feedback overhead. This precoder is created by the BS upon receiving the CSI report through feedback from the UE. This process is depicted in Figure 2.2, where first, the UE selects L best beams from a set of specific RF associated beams (obtained from CSI-RS) and feeds them back to the BS along with their amplitude scaling factors(obtained based on the received power strength) and co-phase factors for the BS to create the final precoder. The codebookConfig part of the CSI report is used to feed back these parameters from the UE to the BS.

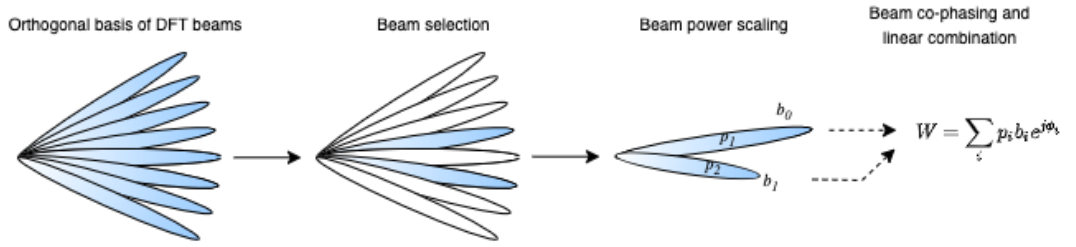

Figure 2.2: *Type II* CSI LC-precoder creation [12].

In Figure 2.2, b_i $(i = 1 : L)$ is the 2D DFT beam which is selected by the UE from the orthogonal basis. p_i is the real-valued wideband power-scaling factor which is a value from the set $[1, \sqrt{0.5}, \sqrt{0.25}, \sqrt{0.125}, \sqrt{0.0625}, \sqrt{0.0313}, \sqrt{0.0156}, 0]$ [1]. The best beam selected by UE (p_1) is always given unity as the power-scaling factor. The received power of the remaining $L-1$ beams selected are compared with that of the best beam and then assigned the nearest value from the above set. A total of three bits are allocated for reporting the p_i in the feedback. A subband amplitude scaling factor can also be included in the linear combination, however, this increases the feedback overhead. $e^{j\phi_i}$ is a complex-valued beam co-phasing factor applied to adjust the different polarisations, where ϕ_i can be a value from the set $[\pi/2, \pi, 3\pi/2, 2\pi]$ or also configured as an 8-Phase Shift Keying (PSK) alphabet (two bits for QPSK and three bits for 8-PSK in feedback).

Type II CSI supports up to rank two transmission layers. The detailed formulae for codebook calculation for higher rank systems and the parameter descriptions can be found in the 3GPP technical specification in [1].

2.3 Social XR application

The term XR encapsulates Augmented Reality (AR), Virtual Reality (VR) and Mixed Reality (MR). VR headsets manifest simulated immersive visual experiences to users. AR applications are increasingly used in modern day gadgets such as smartphones and tablets to enhance user experience by superimposing the digital world with the real environment. MR is a blend of AR and VR technologies. MR devices constantly gather information about the surroundings and use that to allow user interaction upon the real environment in addition to seamlessly placing digital information on top of it. When the aforementioned technologies are linked to a communication platform, the virtual and physical worlds start to merge. A typical example of a Social XR application is when a video call with a colleague transforms to an almost real in-person conversation with a 3D-version avatar of that colleague.

Such enriched applications necessitate high throughput and low latency for seamless video streaming and interactive experiences. [15] and [26] suggest a throughput requirement of 100 Mbps for an entry-level VR application. [2] provides an estimate of 50-100 Mbps and [9] suggests 100-200 Mbps requirement for a common streaming strategy. The throughput requirement for the thesis work is fixed as 100 Mbps.

The PLR is the ratio between the number of lost packets and the total number of generated packets. The thesis considers this as one of the key performance indicators. As per [7], the PLR should not exceed 5 % for a tolerable experience in video streaming applications. Further details of the same are discussed in chapter 3.

2.4 Contributions

As mentioned before, the better the channel knowledge at the BS, the higher the accuracy of beamforming performed at the BS, leading to significant gains in radio performance. The thesis considers TDD systems covering SU-MIMO and MU-MIMO techniques and conducts the performance analysis of Types I and II CSI feedback for a Social XR indoor conference application scenario using the SXRSIM simulator.

The base codebook used for the CSI feedback is 2D-DFT based, where the number of precoders are dependent on the number of AEs in the BS. As a part of understanding configurable parameters of the DFT codebook design, an impact analysis of the pivotal configurable parameter RF is conducted and optimal values are obtained for the indoor XR scenario. Further, we also explore the concept of the 'adaptive-RF' which is found to provide better system performance than the 'fixed-RF' approach. We discuss and detail the trade-offs involved in choosing both aforementioned approaches.

For $Type\ II$ CSI, we further analyse the impact of different linear combination sets of beams ($L = 2$, 3 and 4) reported by the UE on the XR application under consideration. We also compare the $Type\ II$ performance with that of a single beam selection ($L = 1$) in $Type\ I$ CSI. The thesis also investigates the downlink performance of both $single - rank$ and $dual - rank$ cases. In the process, the thesis also proposes an interference estimation mechanism. The thesis attempts to create a similar logic simpler interference estimation model which is based on precoder-aware interference book-keeping. The impact analysis of yet another important configurable parameter called the co-scheduling parameter(γ) is

conducted and the insights are shared.

Both 3.5 GHz and 26 GHz frequency bands are considered for the analysis. Insights on the performance difference between the two frequency bands are detailed. Finally for the ideal configuration combinations, a bandwidth analysis is performed to find the minimum bandwidth requirement for achieving the target PLR performance. Further details of the performance analysis is provided in the modelling and results chapters.

Chapter 3

Modelling

This section covers the integrated modelling framework of the thesis. The Social XR application scenarios, user behavior, radio network deployment and key radio resource management aspects are covered. The CSI codebook modelling is covered in detail for both *Type I* and II CSI techniques.

3.1 Social XR application

The following subsections cover the physical settings, antenna modelling, user behaviour and traffic model of the Social XR use cases considered for the thesis research.

3.1.1 Physical setting

The physical setting under consideration resembles a Social XR conference room, the top view of which is as depicted in Figure 3.1. The number of physical users and virtual users (N_{phy} and N_{vir}) is individually equal to 16. In the conference room of dimensions 10 m $\times$ 10 m $\times$ 3 m, a round table is placed with radius (r_{t}) 2.6 m. The users are uniformly distributed around the table placed at the centre of the room. Throughout the meeting duration, the users remain seated. The user mobility occurs through a head rotation model, the details of which are covered in Section 3.1.3. The BS antenna is located on the ceiling of the room (at a height of 3 m), at the centre, facing downwards.

3.1.2 Antenna modelling

Both 3.5 GHz and 26 GHz spectrum are considered for the thesis. As described by 3GPP in [5], for simulations with a 3.5 GHz carrier, a rectangular BS antenna array consisting of 16 dual polarised AEs (i.e. 4×4 ($\times$ 2)) and with 26 GHz, an antenna array of 64 dual polarised AEs (i.e. 8×8 ($\times$ 2)). A half-wavelength distance is maintained between each pair of cross-polarised AEs as shown in Figure 3.2.

A completely digital beamforming approach is followed where all AEs of the 32T32R and 128T128R antennas are fed by independent RF chains. The maximum transmit power of the antenna is set to 20 dBm [3]. A single TDD carrier of distinct bandwidths (in 3.5 GHz or 26 GHz) is assigned to the BS antenna. A sub-carrier spacing of 60 kHz and an associated slot duration of 0.25 ms is configured, corresponding with 5G numerology 2 (the only numerology present in both sub-6 GHz and mmWave spectrum).

The UEs are incorporated into a Head-Mounted Display (HMD) worn by the user. These

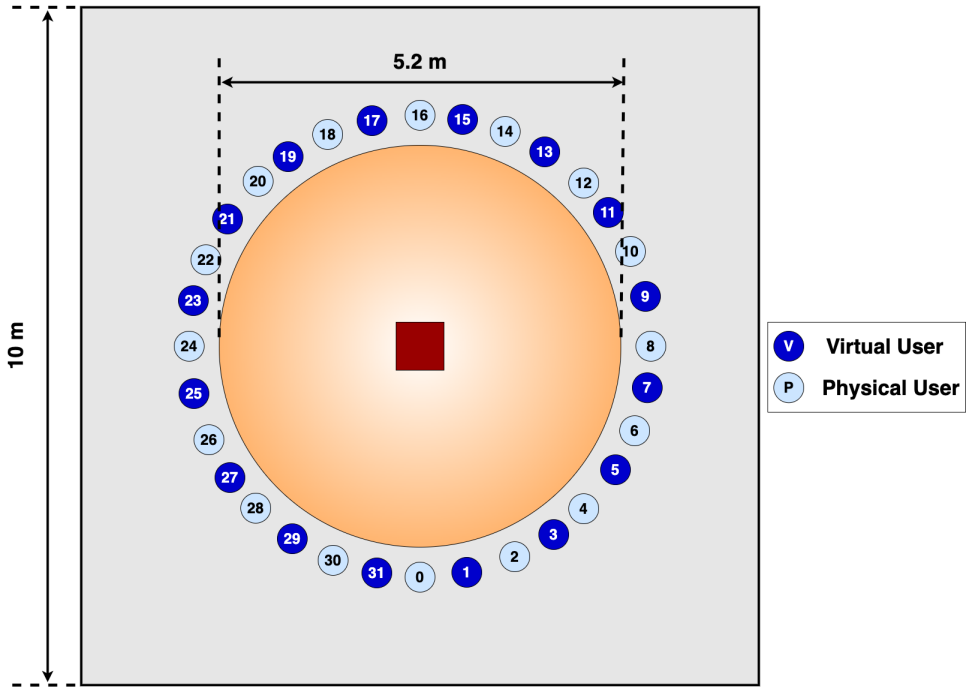

Figure 3.1: Visualization of the 'Social VR' application scenario (top view of the conference room) with 16 physically and 16 virtually present meeting participants.

UE antenna array consists of 2 × 2 and 4 × 4 dual polarised AEs for 3.5 GHz and 26 GHz, respectively with half-wavelength inter-AE spacing, as depicted in Figure 3.2. The noise figure at the UE is assumed to be 8 dB.

3.1.3 User behavior

The dynamics of the meeting are modelled by traversing through a pre-defined speaker list, where each designated participant speaks for a fixed time of τ_s seconds. The thesis considers τ_s as 4 seconds and a total meeting duration of 16 seconds (restricted by computational/storage limitations we try to capture most of the variability using multiple meetings instead of long meeting duration). This means that a total of four participants get to speak in the simulated duration. For the discussed scenario with a total of 32 ($N_{\text{phy}} = N_{\text{vir}} = 16$) participants, the sample speaker list considered includes users 18-22-26-30 considering their positional symmetry across the table. This can be further expanded to include an ideal scenario where each user gets to speak for four seconds. Apart from the changes in the head orientation which occurs due to aforementioned speaker changes, the head position and orientation randomization effectively constitute some degree of 3D 'head wobbling', where the intensity can be configured through the head motion index μ (fixed as 3 in our case). The changes in the position and orientation of a UE's head also directly affect the position and orientation of the UE's antennas which in turn affects the downlink channel quality due to multipath fading.

As mentioned before, each user who is physically present in the conference room remains seated in their respective chair throughout the meeting duration. The mobility of the user is through randomized head motion resulting in a change of head position and orientation [13][16]. Since the UE antennas are fixed to the VR headset of the user, the user's head

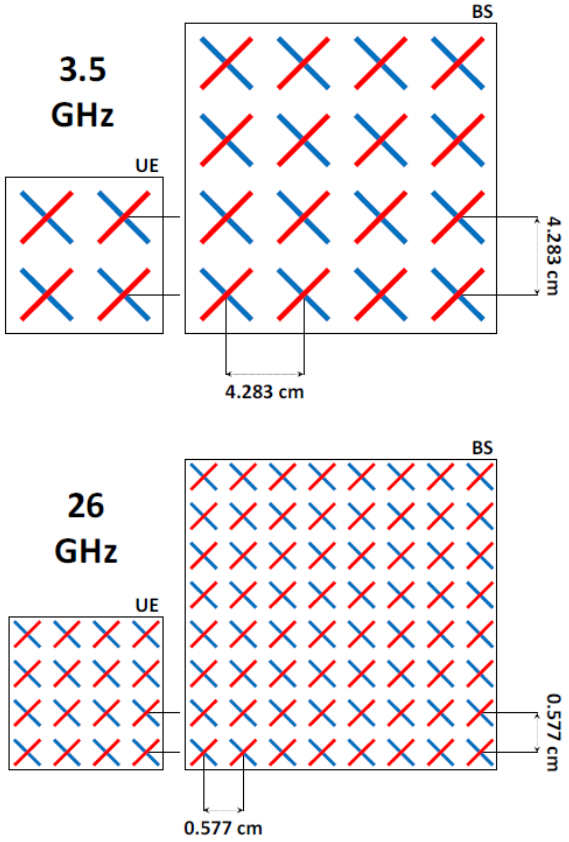

Figure 3.2: Assumed UE (HMD; left) and BS (right) antenna arrays for the 3.5 GHz (top) and 26 GHz (bottom) scenarios [30].

movements directly impact the position and orientation of the mounted antennas. The mobility model can be viewed as a combination of position and orientation of the user's head [30].

Position: The head's position is modelled according to a modified random 3D way-point model [30]. The average (or default) head position is marked with coordinates (x_0, y_0, z_0), where (x_0, y_0) is given by the respective user's chair position and z_0 is fixed to 1.4 m. The initial position of the head is sampled according to a 3D Gaussian distribution with mean vector (x_0, y_0, z_0) and standard deviations $(\sigma_x, \sigma_y, \sigma_z)$ (0.667 m, 0.667 m, 0.223 m). The respective co-variances are set to 0 m^2. Sampled from the same distribution, the head is modelled to move linearly from the initial position to its next, at a speed of $0.1 \times \mu$ m/s, where μ is the head motion index in the range [0, 10]. This process repeats itself till the end of the meeting duration. The thesis considers a μ value of 3 constituting a head movement speed of 0.3 m/s.

Orientation: The orientation of the user's head is defined by a randomly sampled 3D vector with angular offsets around a straight line aimed at the current speaker (the speaker himself is assumed to aim his view at the previous speaker). These offsets are independently sampled with respect to the pitch, yaw and roll axes perpendicularly cutting across the user's head, and assume uniform angular distributions on the ranges $[-\alpha_P, \alpha_P]$, $[-\alpha_Y, \alpha_Y]$ and $[-\alpha_R, \alpha_R]$, respectively, with $\alpha_{P/R} = 10°$ and $\alpha_Y = 20°$. Whenever the switch between the speakers happens, the sampling of the offsets occur and the corre-

sponding change in orientation modelled takes place in $1.5 - 0.2 \times \mu$ seconds, with μ as defined and configured above. When the target orientation is reached, a new offset is sampled and the process is repeated for the duration of the meeting.

3.1.4 Traffic model

The traffic model for the Social XR application considered resembles that of a persistent real-time User Datagram Protocol (UDP)-based video streaming, where the upstream or downstream is a sequence of Group of Pictures (GoP). A GoP is essentially a series of frames arranged into a sequence. Considering the size of GoP to be M_{GoP}, a GoP contains one intra-coded frame (I frame) and $M_{\mathrm{GoP}} - 1$ predictive-coded frames (P frames). I frames indicate the start of a GoP and constitute the complete picture and P frames are considerably smaller frames which are dependent on the previous frames within the same GoP and hence are more compressible than I frames. The application-level bit rate R_{B} (in Mbps) is given by Equation (3.1) where the size of an I frame is denoted by S_{I} (1250000 bytes), the size of a P frame denoted by S_{P} (250000 bytes), the frame generation rate is denoted by R_{F} (30 frames per second) and $S_{\mathrm{I}} > S_{\mathrm{P}}$. Figure 3.3 shows the VR application traffic model for $M_{\mathrm{GoP}} = 6$.

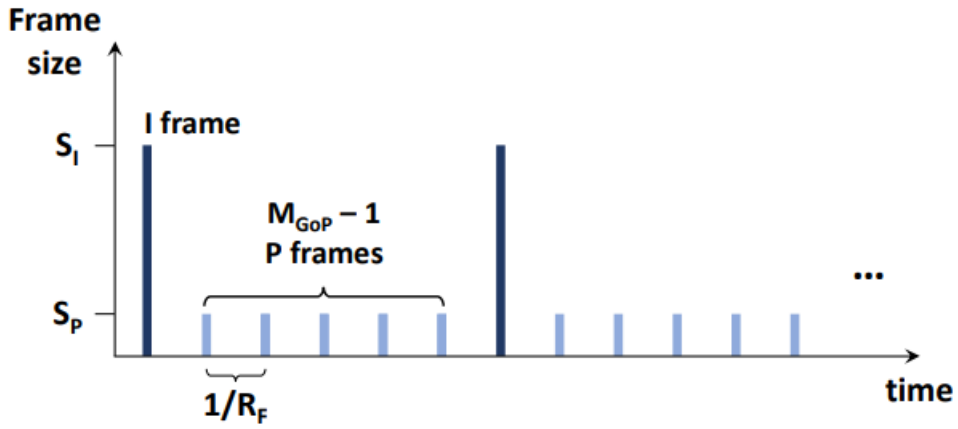

Figure 3.3: VR application traffic model for GoP size 6 [30].

$$R_B = \frac{8\ R_F(S_I + (M_{GoP} - 1)\ S_P)}{10^6\ M_{GoP}} \tag{3.1}$$

The video information which is generated as application-level frames at the source, arrives in the form of 1500-byte IP packets at the BS transmission buffer. The packet latency variabilities on the downstream path from source to BS transmit buffer cause the temporal dispersion of packets. The downstream time dispersion is modelled as follows [30]. When the video frame is generated, the frame is segmented into IP packets at a 'packet extraction bit rate' given by $R_{\mathrm{B}}/(1–\beta)$, with the application-level bit rate R_{B} and the configured burstiness parameter $\beta \in [0, 1]$. For $\beta = 0$, the IP packets are maximally dispersed (effectively yielding a constant bit rate flow), and scenarios where β approaches unity ($\beta \longrightarrow 1$), each video frame is instantaneously segmented into IP packets upon generation, which reflects the maximum degree of burstiness. The thesis assumes a β of 0.5 for the simulations. The impact of β on the traffic profile is shown in Figure 3.4.

Considering the application as 'conversational video (live streaming)', the QoS requirement

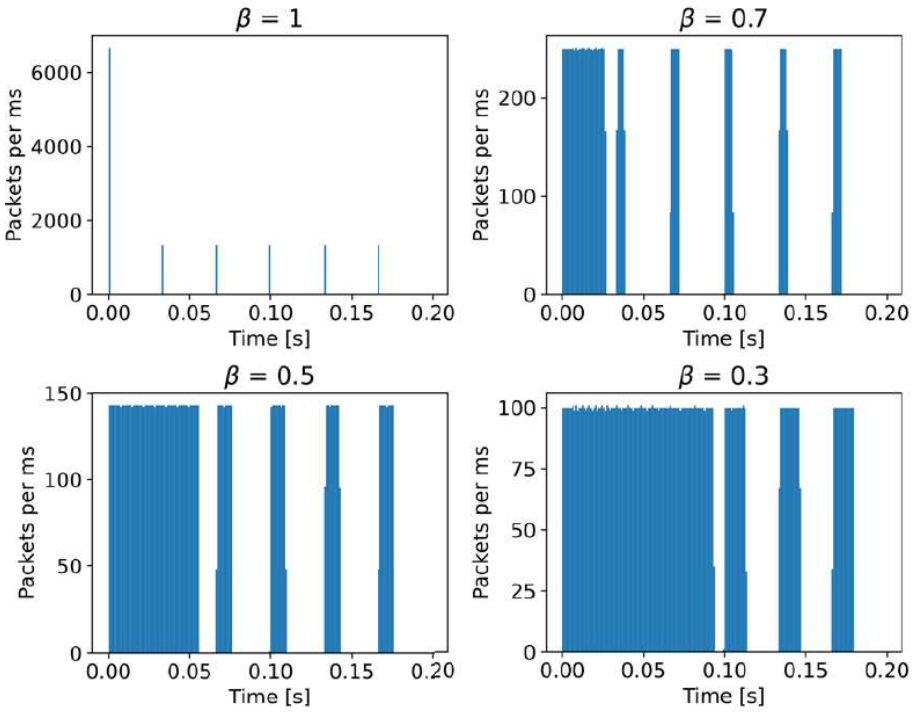

Figure 3.4: Packet arrival traces for scenarios with $M_{\text{GoP}} = 6$, R_{B} =100 Mbps and different burstiness values β [30].

of the VR application is specified by a maximum tolerable end-to-end one-way frame-level latency of Δ_{E2E} (a constant offset away from Δ_{RAN}, we drop packets based on the Δ_{RAN} value of 10 ms, so we do not specify a value for Δ_{E2E} for our scenario). A VR frame which is delivered with a latency exceeding Δ_{E2E} is considered useless. The thesis assumes that the external network uses part of this end-to-end budget, and the remaining part is the packet-level budget for the RAN segment of $\Delta_{\text{RAN}} < \Delta_{\text{E2E}}$ ms, acknowledging that the IP packets are handled by the RAN which is unaware of application-level video frames [26]. The packet scheduler which will be detailed in Section 3.2.2, uses Δ_{RAN} to set due priority to packets approaching the associated transmission deadline and also drop packets that (are estimated to) exceed the deadline. The Δ_{RAN} value of 10 ms is considered for the thesis.

3.2 Propagation modelling

Channel modelling can be performed through deterministic and stochastic approaches. While stochastic approaches are based on channel measurements, deterministic methods use ray-trace-like approaches to build a better channel model compared to its counterpart, bearing the cost of high computational demand and complexity. QUAsi-DeteRministic RadIo channel GenerAtor (Quadriga) is an open source channel model generator which follows a geometry-based stochastic channel modelling approach [11]. A set of features in the model also help to enable quasi-deterministic multi-link tracking of users in different environments. Thus, the model can be considered as a good blend of aforementioned approaches.

The propagation environment characteristics with respect to path loss, shadowing and

multi-path fading follow the 3GPP line-of-sight 'indoor office' scenario specified in [5] with implementations provided by Quadriga [11] (also for the Quadriga NLOS model, the same modelling and results hold, since at the considered short tx-rx distances, the LOS component is rather dominant.). Each trace contains complex impulse response between the UE and the BS antenna pair, which takes into account the path loss, our scenario specific fading and the antenna orientations. Blockage is not considered, however a detailed study of the same has been conducted and a state-of-the-art generic blockage model has been proposed as part of internship study in [21]. Quadriga does not take noise into account, hence we add a thermal noise power (P_{N}) which is calculated using the Equation (3.2), where the Boltzmann constant $k_{\mathrm{B}} = 1.380649{\times}1023$ J/K, temperature $T = 290$ K and frequency bandwidth B.

$$P_N = k_B T B \tag{3.2}$$

3.3 Radio resource management

At the UE side, receive beamforming is used in the form of Maximum Ratio Combining (MRC). The downlink 'beam pair' is a combination of a selected CSI-RS beam (or a linear combination of multiple CSI-RS beams) and a selected MRC configuration at the UE receiver. The BS periodically (with configurable periodicity parameter τ_{CSI}) transmits CSI-RSs and the UE measures these CSI-RS, derives its CSI feedback and signals this back to the BS, involving a 5-TTI feedback delay. There are two types of CSI feedbacks based on whether the UE sends information about single best beam (*Type I* CSI with $L = 1$) or the information to create an LC precoder combining multiple beams (*Type II* CSI with L =2, 3 or 4). Both *Type I* and *Type II* CSI feedback methods and the base-codebook modelling are detailed in Section 3.3.1.

3.3.1 CSI codebook modelling

This thesis analyses both SU-MIMO and MU-MIMO technologies for single and dual transmission ranks. Both *Type I* and *II* CSI precoding techniques are considered for the aforementioned Social XR scenario. The precoders of the base codebook exhibit DFT characteristics. The RF is an important configurable parameter of the DFT-based codebooks. To understand the significance of choosing the right RF factor, a useful experiment is to observe the system performance for different RF-associated beams as experienced by each participant. From the literature, it is not clear whether single RF-associated beams are sent to all UEs from which the UEs pick the best beam suitable for them (we refer to this as the 'fixed-RF' case) or if every UE is individually allowed to pick the best-suited RF (we refer to this as adaptive-RF scenario). The 'adaptive-RF' case would require a much larger set of CSI-RSs to be broadcast, which may in turn mean that they are sent less frequently or impose more overhead (in terms of consumed resources). We model both 'fixed-RF' and 'adaptive-RF' cases and compare the performance and trade-offs. Chapter 4 elaborates on the results and analysis of the same.

DFT codebook

The frequencies considered for the thesis study are 3.5 GHz and 26 GHz. The codebook parameters depend on the antenna configurations, which in-turn depend on the frequency used. The detailed values are described below.

3.5 GHz: The configuration of the DFT codebook for the URA type antenna at the

BS depends on the number of dual-polarised antennas. For 3.5 GHz, a rectangular BS antenna array consisting of 16 dual polarised AEs (i.e. 4×4 ($\times$ 2)) is used, making $N_1 = N_2 = 4$. For this value set, 3GPP [1] recommends DFT oversampling values of $O_1 = O_2 = 4$. The codebook for this scenario $W_{\text{dual pol}}$ is created using Equation (2.7), where a total of 256 ($N_1 N_2 O_1 O_2$) precoders are generated. The total length of each precoder is 32 ($2N_1 N_2$), of which the first 16 weights are applied to the AEs of the first polarisation and the next 16 applied to the AEs of the second polarisation. The codebook can be segregated into 16 orthogonal grids of beams grouped under 16 different RFs and with each RF containing 16 precoders which are mutually orthogonal. The RFs and their contained precoder column numbers are shown in Table 3.5 and the angle span of the each of the precoders differently color-coded for different RFs are shown in Figure 3.6. Each data point maps to a beam pointing angle in terms of azimuth and elevation angles.

R1	R2	R3	R4	R5	R6	R7	R8	R9	R10	R11	R12	R13	R14	R15	R16
1	2	3	4	17	18	19	20	33	34	35	36	49	50	51	52
5	6	7	8	21	22	23	24	37	38	39	40	53	54	55	56
9	10	11	12	25	26	27	28	41	42	43	44	57	58	59	60
13	14	15	16	29	30	31	32	45	46	47	48	61	62	63	64
65	66	67	68	81	82	83	84	97	98	99	100	113	114	115	116
69	70	71	72	85	86	87	88	101	102	103	104	117	118	119	120
73	74	75	76	89	90	91	92	105	106	107	108	121	122	123	124
77	78	79	80	93	94	95	96	109	110	111	112	125	126	127	128
129	130	131	132	145	146	147	148	161	162	163	164	177	178	179	180
133	134	135	136	149	150	151	152	165	166	167	168	181	182	183	184
137	138	139	140	153	154	155	156	169	170	171	172	185	186	187	188
141	142	143	144	157	158	159	160	173	174	175	176	189	190	191	192
193	194	195	196	209	210	211	212	225	226	227	228	241	242	243	244
197	198	199	200	213	214	215	216	229	230	231	232	245	246	247	248
201	202	203	204	217	218	219	220	233	234	235	236	249	250	251	252
205	206	207	208	221	222	223	224	237	238	239	240	253	254	255	256

Rotation factor
Precoder column in codebook matrix.

Figure 3.5: RF and the associated precoder columns from the codebook matrix for $N_1 = N_2 = 4$.

26 GHz: For 26 GHz, a rectangular BS antenna array consisting of 64 dual polarised AEs (i.e. 8×8 ($\times$ 2)) is used, making $N_1 = N_2 = 8$. For this value set, there is no 3GPP recommendation for DFT oversampling values (3GPP considers sub-arrayed antenna models for 26 GHz frequency band, which would then mean that $N_1 = N_2 = 4$ configuration will suffice, in our thesis we do not consider sub-arraying for 26 GHz.), hence we go with the same set of oversampling values used for 3.5 GHz scenario which is $O_1 = O_2 = 4$. The codebook for this scenario $W_{\text{dual pol}}$ created using Equation (2.7), generates a total of 1024 precoders. The total length of each precoder is 128 ($2N_1 N_2$), of which the first 64 weights are applied to the AEs of the first polarisation and the next 64 applied to the AEs of the second polarisation. The codebook can be segregated into 16 orthogonal grids of beams grouped under 16 different RFs and each factor contains 64 precoders which are mutually orthogonal. The RFs and their contained precoder column numbers are shown in Figure A.1 in the Appendix, the angle span of the each of the precoders differently color-coded for different RFs are shown in Figure 3.7.

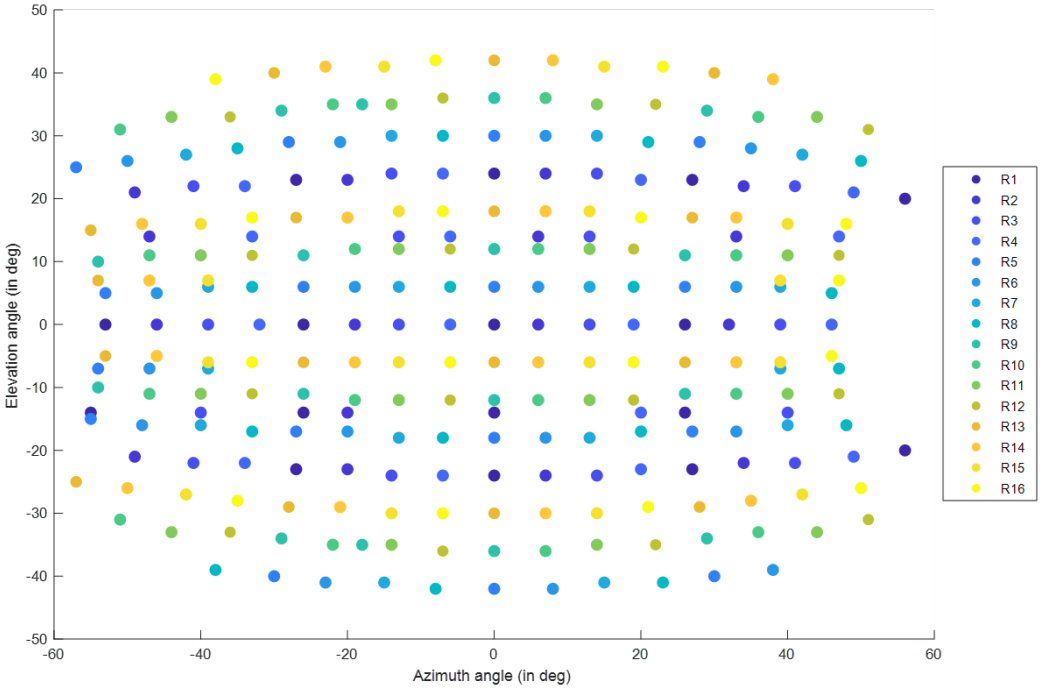

Figure 3.6: RF and the associated precoder angular span for $N_1 = N_2 = 4$.

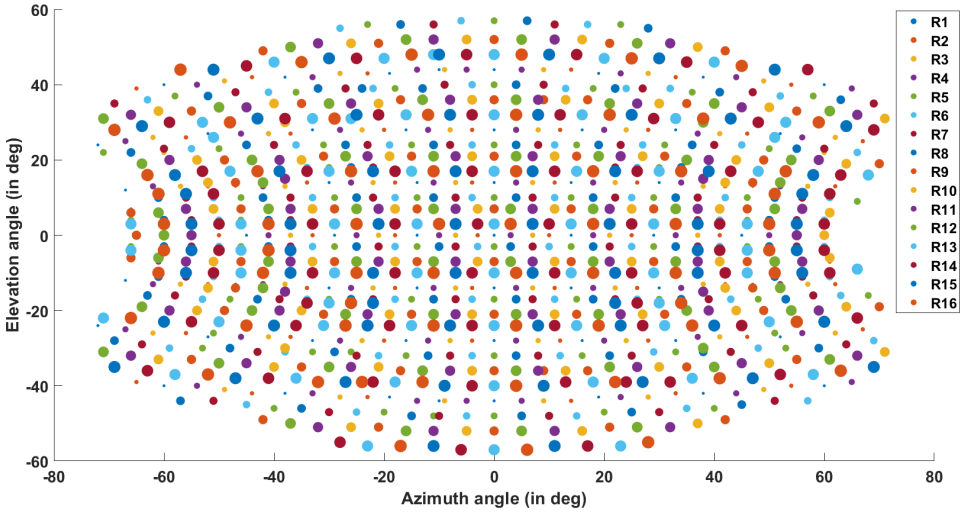

Figure 3.7: Angular span of RF-associated beams from the codebook matrix for $N_1 = N_2 = 8$.

Type I CSI codebook

For the analysis of *Type I* codebook-based CSI acquisition for $single - rank$ transmission, each user present in the conference selects a single best precoder from the above RF-associated beams. The CSI report will convey the details of the same as explained in Chapter 2. For the $dual - rank$ case, the UE chooses two different beams from the

same RF-associated beams. Choosing different beams from the same RF factor reduces the inter-layer interference since orthogonality is maintained between any two beams of an RF factor.

Type II CSI codebook

Type II performs a weighted linear combination of a selected group of precoders from the DFT codebook. As discussed before, the RF-associated orthogonal beams are sent to each UE using the CSI-RS signals and the UE selects L best beams suitable for downlink transmission instead of one beam. For *Type II*, the possible values of L are (2, 3 or 4). We can see that when the value of L is unity, the equation representing *Type II* CSI in Figure 2.2 reduces to *Type I* CSI.

In Chapter 4, we will compare the performance of the system using simulations for the considered Social XR conference for all possible values of L. The strongest beam selected by the UE is given real-valued power-scaling factor p_1 as unity, the received power of the remaining beams are individually divided by the received power of the best beam and the obtained value is rounded to the nearest value in the set $[1, \sqrt{0.5}, \sqrt{0.25}, \sqrt{0.125}, \sqrt{0.0625}, \sqrt{0.0313}, \sqrt{0.0156}, 0]$ to obtain their respective p_{i}. The thesis does not consider the sub-band amplitude power-scaling factor since this adds up to the feedback overhead and is an optional feature.

For the $dual - rank$ case with *Type II*, the thesis considers a heuristic distribution of precoders to the two layers of each UE, for the creation of the final LC precoders. We follow two rules of thumb for this distribution. Firstly, a precoder is allocated to the layer which so far contains the lowest number of precoders. The second rule applies if both layers contain the exact same number of precoders, and in that case, the precoder gets added to the layer that maximizes its power-scaling factor. This is continued until either L precoders are added to each layer or the number of significant power-scaling factor-allocated beams gets exhausted for the specific UE. For example, let's assume that there are four precoders (p_1, p_2, p_3 and p_4) suitable for UE_1 with respective received signal powers (s_1, s_2, s_3 and s_4). For the $dual - rank$ case with $L = 2$, first p_1 is assigned to the first layer. Now as per the first rule, p_2 is added to the second layer. At this point, both layers contain same number of precoders (one each), hence following the second rule, p_3 is added to the layer attributing more power-scaling factor (the power scaling is defined with respect to the received signal power of the strongest beam in respective layers: s_3/s_1 and s_3/s_2) to it (let's say, the second layer in this case). p_4 is then automatically assigned to the first layer as per the first rule.

3.3.2 Scheduling

The resources configured by an applied TDD duplexing scheme are configured by a frame size of five time slots and a fixed UL/DL resource split of 1:4. For the downlink slots, all symbols are used for DL transmission. However, the 3GPP recommended control signaling overhead of 14% and 18% when using a 3.5 GHz and 26 GHz carrier, respectively [4], is also considered while calculating the downlink radio efficiency for obtaining the bit rates.

Compute UE Priorities with Scheduler

The scheduler used in the thesis is the Modified-Largest Weighted Delay First (M-LWDF) packet scheduler. The M-LWDF is a latency-oriented packet scheduler modelled to govern wideband-based downlink transmissions [8]. In case the head-of-line packet is determined to not to meet the aforementioned RAN-oriented packet-level latency budget Δ_{RAN}, it is dropped from the transmit buffer. Recall that the reasons why incurred delays may be so high that a packet is indeed dropped can be attributed to three distinct reasons. (i) due to too many block errors and consequent re-transmissions; (ii) due to poor channel quality and consequently poor bit rates; and (iii) due to congestion in relation to other traffic.

At each scheduling opportunity (basically i.e. at each Transmission Time Interval (TTI); taken equal to a time slot), the M-LWDF scheduler ranks the UEs based on priority levels calculated using Equation (3.3). Only UEs with non-empty buffers are considered to be part of the scheduled list. For UE i at TTI t, the scheduling priority is given by Equation (3.3), where $W_{\mathrm{i}}(t)$ denotes the flow's experienced head-of-line packet latency, $R_{\mathrm{i}}(t)$ denotes its instantaneously attainable bit rate and $\hat{R}_{\mathrm{i}}(t-1)$ indicates the exponentially smoothed bit rate it experienced so far.

$$P_i(t) = -\frac{log_{10}\delta_i}{\Delta_{RAN}}\ W_i(t)\ \frac{R_i(t)}{\hat{R}_i(t-1)} \tag{3.3}$$

The UE priority also depends on the number of layers co-scheduled, since that affects the transmit power, the estimated SINR and the selected MCS and hence the $R_i(t)$ in the numerator. The expected SU-MIMO bit rate for the $single-rank$ case is compared with that of the $dual-rank$ case and the highest bit rate is used to calculate the UE priority in Equation (3.3).

Co-scheduling multiple layers

For MU-MIMO scenarios, after the priorities of the UEs are calculated, the decision for co-scheduling multiple layers (which may target different users) is made by scheduling the first UE in the ranked list and then updating the list with the remaining layers when they pass the orthogonality check (detailed below) with respect to the already scheduled layers in the list.

The decision for co-scheduling of multiple layers, which may target the same or different users, is based on the extent of overlap of the main lobe of the selected beams. This extent can be determined by an orthogonality check between the finally selected precoder of the UEs (single precoder in case of $Type\ I$ CSI and the final LC-precoder in $Type\ II$ CSI). The degree of orthogonality is determined by complex dot product of the precoder weights, which is compared with the co-scheduling threshold $\gamma \in [0, 1]$. We introduce gamma $\gamma \in (0, 1)$ as the co-scheduling parameter. While comparing the beams selected for possible co-scheduling, the value zero for the co-scheduling parameter indicates that the beams selected by the respective UEs are perfectly orthogonal and hence they can be co-scheduled. In the event of maximum possible interference or overlap between the selected beams, the co-scheduling parameter value of unity is obtained. The smaller the co-scheduling parameter, the lesser the overlap and thus, smaller the interference. Figure 3.8 shows the polar plots of precoded beams of two layers with the overlap and respective γ values. The impact of different γ on the system performance is analysed in detail in Chapter 4.

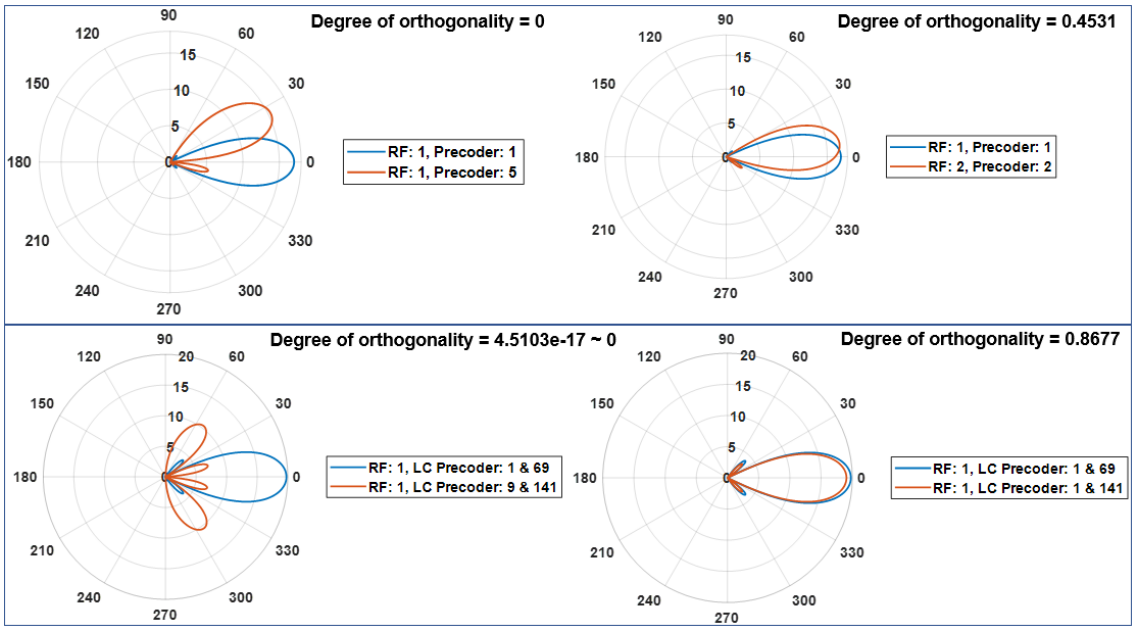

Figure 3.8: Top set contains polar plots of two precoded beams (each with L = 1), left image: both precoders are chosen from the same rotation factor with dot product = 0. Right image: Each precoder belongs to a different RF with dot product = 0.4531. Bottom set contains polar plots of two LC precoded beams (each with L = 2), left image: both beams of L2 are differently chosen from the same rotation factor with dot product = 4.5103e-17 $\sim$ 0. Right image: First beam (best beam) of L2 are common and second beam is differently chosen from the same rotation factor with dot product = 0.8677.

Interference estimation

We need to estimate the interference the scheduled transmission will experience in order to select the most suitable MCS for the transmission.This thesis deals with single-cell scenarios and from the existing literature on intra-cell downlink interference estimation techniques, one of the relevant recent studies in [10] proposes an estimation technique based on geometric Multi-elliptical Propagation Model (MPM) which is shown to be an effective approach.

While the CSI-RS reference signals used to measure the channel are known as non-zero power (NZP) CSI-RS, it is also possible to configure a zero power (ZP) CSI-RS. These CSI-RS occupies the configured resource element (RE), but the BS does not transmit any energy in these REs, making them empty. The ZP CSI-RS can be used to define an interference measurement resource (CSI-IM), i.e the UE measures the interference from on-going transmissions without measuring the received power of its own [12]. This is how we assume the BS knows the experienced interference of the UEs. The thesis uses a simplified precoder-aware interference estimation mechanism in which we keep a track of realised interference per UE for every new combination of UEs scheduled and respective precoders used. When such a tracked combination occurs again, we use the realised interference recorded previously as the estimated interference for the present TTI. Since the UEs are seated for the entire conference duration and the mobility is restricted to only the head movements, we find this method to be effective, since we observe that the precoders used by the UEs are constant throughout the conference. Whenever a new combination

of scheduled UEs and applied precoders arises, for which there is no tracked interference data, the realised interference of the previous TTI is used. In case the UE was not served in the previous TTI, the estimated interference for the UE for the previous TTI is used.

Bit rate estimation

For the estimation of the instantaneous bit rates of the UEs, an SINR estimation based on the last reported CSI is performed. This estimated SINR is then used to calculate the CQI from the BLock Error Rate (BLER) curves (Figure B.1 in Appendix B). The highest CQI corresponding to the estimated SINR is chosen, such that it achieves a BLER lower than the target BLER of 10%. This determines the MCS selection for the transmission. The selected MCS defines the code rate R_{c} and thereby the contained number of bits in a symbol N_{bits}^{Symbol} bits. The attainable bit rate R in bit/s is computed as shown in Equation (3.4), where N_{Symbol}^{PRB} represents the number of resource elements used for data (168 in our case). T_{TTI} represents the slot duration, the value of which depends on the configured numerology (0.25 ms for the 5G numerology of two) The bit rate is used for computing UE priorities, in case a channel-aware packet scheduler is configured.

$$R = \frac{R_c N_{bits}^{Symbol} N_{Symbol}^{PRB}}{T_{TTI}} \tag{3.4}$$

In a given TTI, the transmitted data is split into multiple Transport Blocks (TBs). For every TTI, we consider a fixed number of TBs ($N_{\mathrm{TB}} = 5$). A BLER-based coin is flipped (which is based on the applicable BLER curves with the realised SINR and the estimated MCS) to decide the successful transmission of a TB. The realised SINR is determined by the use of a the Mutual Information Effective SINR Mapping (MI-ESM), which aggregates the SINRs over all the PRBs into one effective SINR ([29]). In the event of a successful transmission, the buffers are updated and the bits are removed. Once all the bits of the packet are sent successfully, the last transmission timestamp is recorded as the final arrival time for that packet.

3.4 Simulator

The objective of the thesis could also be achieved through modifications on existing fully working system-level simulators, provided they are feasible with the Social XR scenarios under consideration. NYUSIM simulator detailed through [37] covers only outdoor environments and hence does not suit our requirement. Another well known simulator is the Vienna simulator detailed in [32]. This simulates the downlink in generic indoor environments and is also compatible with Quadriga channel model. *Type I* CSI is already implemented in the simulator. Another simulator suited for the study involving indoor environment and XR scenarios is the Social XR simulator modelled by TNO in [30]. Since the thesis is done in collaboration with TNO, we model the thesis using the Social XR simulator, where Quadiga is used to generate channel traces, which are than read into the system-level simulator..

Chapter 4

Results and analysis

The purpose of this chapter is to investigate how the performance of the Social XR use case described in Chapter 3 varies with different frequency bands, CSI feedback techniques, RFs, MIMO techniques, transmission ranks and γ values using the Social XR simulator. Table 4.1 summarises the important configurable parameters used in the simulation, along with their symbols and considered values.

Parameter	Symbol	Value
Number of participants	N_{phy}, N_{vir}	16
Frequency band	f	3.5 GHz, 26 GHz
Motion index	μ	3
Application bit rate	R_B	100 Mbps
RAN latency budget	Δ_{RAN}	10 ms
CSI periodicity	τ_{CSI}	5 ms
CSI acquisition techniques	-	Type I, type II CSI
Type II CSI number of beams	L	2, 3, 4
Number of dual pol. antenna sets	N1, N2	(4, 4 for 3.5 GHz), (8, 8 for 26 GHz)
Codebook oversampling factors	O1, O2	4, 4
Rotation factor	RF	1-16
Co-phase factor	φ	$\pi/2$
MIMO techniques	-	SU-MIMO, MU-MIMO
Transmission ranks	-	1, 2
Carrier bandwidth	-	400 MHz
Numerology	-	2
Burstiness parameter	β	0.5
Co-scheduling parameter	γ	{0, 0.2, 0.4, 0.6, 0.8, 1}

Figure 4.1: Configurable parameters and their values used in simulation.

The thesis considers PLR as the **key performance indicator**. The PLR is obtained by taking the ratio of total number of lost packets to the total number of generated packets for a given flow (or user). As mentioned in Chapter 2, a PLR of 5% is considered as the maximum limit for a tolerable XR performance.

For each scenario presented in the following sections, a set of five meetings are simulated, where every meeting has a random channel initialization. The meeting duration is

set to 16 seconds which provided sufficient PLR convergence. The performance analysis of 3.5 GHz and 26 GHz are detailed separately in the Sections 4.1 and 4.2. A confidence interval of 95% is considered for the provided data and marked in the presented charts in the Sections 4.1 and 4.2. The narrow confidence intervals observed during the measurements prove the sufficiency of the chosen number of five meetings for the simulations.

4.1 Performance analysis for 3.5 GHz

This section details the observations and analysis of the results pertaining to the 3.5 GHz frequency band. The performance comparison of the 'fixed-RF' and 'adaptive-RF' is elaborated in section 4.1.1. Sections 4.1.2 and 4.1.3 contain the performance analysis of SU-MIMO and MU-MIMO technologies when $Type$ and $Type\ II$ CSI feedback methods are used for different values of γ and transmission ranks. Behind the average PLRs (averaged across UEs and simulated meetings) we observed some variability between the UE-specific PLRs. However, to assess the first order effects of these configuration options, we focus on the average PLRs in the presented charts and results. Also, it should be noted that the term $dual-rank$ (used extensively throughout the results (Chapter 4) and conclusion (Chapter 5) does not mean dual rank transmissions but the ability of the UE to give ($single-$ or) $dual-rank$ CSI feedback and of the scheduler to select ($single-$ or) $dual-rank$ transmissions.

4.1.1 Fixed-RF and adaptive-RF

As detailed in the Section 2.2.2 of Chapter 2 and Section 3.2.1 of Chapter 3, each individual RF contains a grid of orthogonal beam sets spanning different azimuth and elevation angles. The best beam (or beam combination for an LC precoder) suitable for a UE can belong to any of the 16 different RF present in the CSI codebook. It should be noted that the ideal precoder for different UEs can belong to same or different RF factor. Hence the choice of RF can significantly affect the system performance since a sub-optimal RF can result in sub-optimal beam for a UE and hence affects the downlink performance. In Figure 4.2 we make a distinction between the 'fixed-RF' and 'adaptive-RF' cases, where in the former all the UEs are served with single best beam ($L = 1$) from each of the 16 RFs and in the latter each UE individually picks the RF (and thereby the best beam ($L = 1$)) best suited for it. The provided PLRs are insensitive to any setting of the co-scheduling parameter γ value except unity for the 'fixed-RF' case with $L = 1$, since the beams within an RF are mutually orthogonal by design, and a collision can only occur if two UEs select the exact same beam from the RF's GoB.

We can observe that the PLR varies significantly over the 16 RFs for the 'fixed-RF' case. This is in accordance with the specific location of the UEs with respect to the point in space where the beams of the serving 'fixed-RF' are spanning (the spanning angles of different beams of RFs 1-16 are shown in Figure 3.6). For example, if the UE (or the antenna) would be moved a little bit to the left (or right), a different 'fixed-RF' may serve the UE best. If an an operational setting, if 'fixed-RF' applies, then the selected RF may be rather arbitrarily set, since the operator has of course no idea where people are located at any given point of time and it is unlikely that the best RF (red bar demarcated RF: 3 in this case) will be selected. Through this chart we understand how 'good' or bad it can get, if the operator decides to go for a 'fixed-RF' setting.

It would be ideal if the RF is not fixed and every UE gets to pick the best RF and thereby the best beam suitable for it regardless of the choice of other UEs. This method (referred to as adaptive-RF in the thesis) would definitely give better system performance as shown by the green bars in Figure 4.2. The PLRs for the 'adaptive-RF' case vary with the γ value since adaptive-RF span over all RFs and hence the beams picked by different UEs may not be always orthogonal like for the 'fixed-RF' case. It is evident that while the lowest PLR observed out of all the 'fixed-RF' cases (color-coded as red and RF: 12) is marked at 12.24%, the maximum PLR found for the 'adaptive-RF' case is 5.64% for γ values greater than or equal to 0.8. The lowest PLR found for the 'adaptive-RF' case is 0.01%, which is well below the assumed maximum tolerable PLR for XR application.

From the literature it is not clear whether a fixed or adaptive-RF is adopted in real-life deployments. Hence we analyse the performance of both methods through this experiment. While the 'adaptive-RF' outperforms the 'fixed-RF' case for the considered XR scenario, there is a trade-off involved in choosing adaptive-RF over fixed-RF, which is the requirement of a much larger set of CSI-RSs to be broadcast comparatively, which implies that they are either sent less frequently or impose more overhead (in terms of consumed resources). For the present scenario, since the UEs movement is restricted to head rotations (which means that the UEs mostly stick to same precoders throughout the meeting duration), a less frequent CSI-RS for 'adaptive-RF' case should hardly impact the performance.

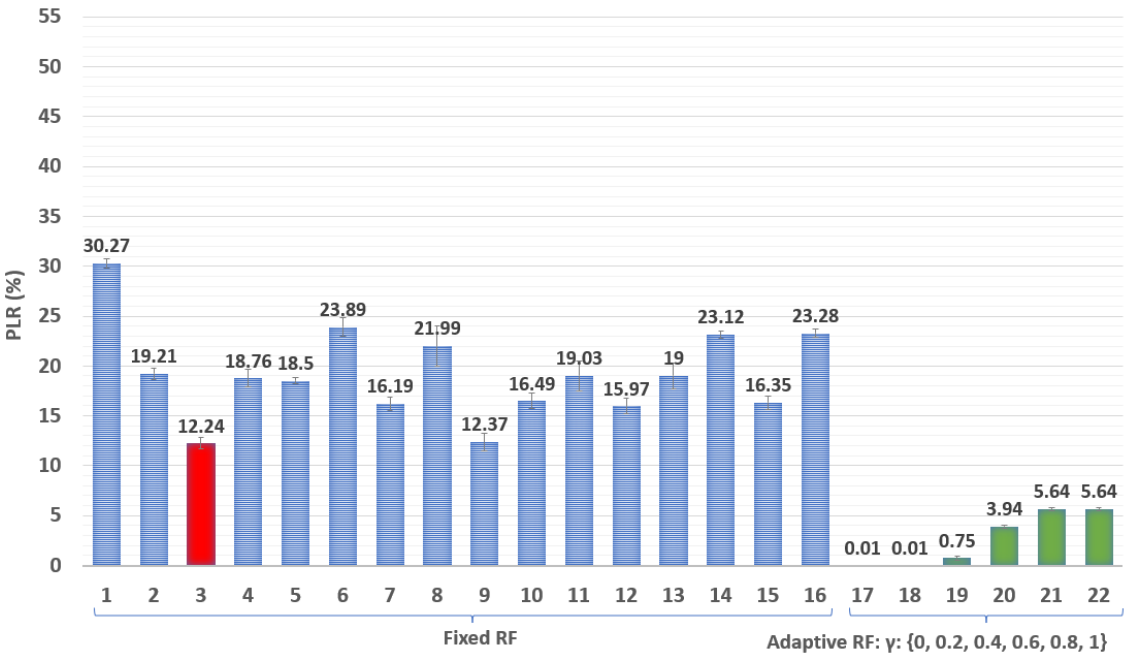

Figure 4.2: Average PLR across all UEs and simulated meetings for comparing the system performance when fixed-RF and adaptive-RF are used for 3.5 GHz. The blue bars show the PLR when all UEs select their precoders from a fixed-RF (1-16) (with the red bar indicating the best fixed-RF 3) and the green bars show the PLR when the UEs use adaptive-RF and individually select the best RF for different γ values. A confidence interval of 95% is marked on each data bar, the small confidence interval observed prove the convergence of PLRs for the number of meetings simulated.

4.1.2 Impact of Type I and Type II CSI on SU-MIMO technology

Figure 4.3 shows the downlink performance for the XR environment when SU-MIMO technique is used. Since only a single user is scheduled in any given TTI, a single-user scheduler does not have the γ parameter. It should be noted that SU-MIMO is not simply the same as MU-MIMO with $\gamma = 0$, since a zero value of γ could still refer to MU-MIMO with zero estimated interference between the co-scheduled UEs. The chart (and the remaining 'fixed-RF' charts for both frequency bands) shows that for the 'fixed-RF' case, PLRs that are well above the said requirement (5%). The observed PLRs may be interpreted as such, assuming that in reality the application layer would respond to such high experienced PLRs by lowering the codec rate. Also, note that the cross-layer frame type-based scheduling (i.e. giving some degree of priority of I-frame packets over P-frame packets) may yield acceptable QoS even for relatively high PLRs [14].

For the $single-rank$ case, we observe that each UE achieves the maximum MCS possible in the considered indoor conference scenario, owing to the full transmit power of the BS being assigned to the UE (compared to the MU-MIMO case where transmit power gets divided by the number of UEs co-scheduled) and complete absence of interference. The reason for the PLR of 21.52% despite of achieving highest MCS possible, is the reduced number of times each UE is scheduled (once every 16 TTIs). For the same reason, we see the same average PLR for both $Type\ I$ and $Type\ II$.

For the $dual-rank$ case, it is not always the highest MCS that is selected every TTI for each UE, since the transmit power per layer is half of the BS transmit power and also there is some inter-layer interference present in case the scheduler indeed decides to co-schedule multiple transmission layers. With the error bars taken into consideration, we observe that the $dual-rank$ PLR performance is similar for different L values and also matches the $single-rank$ PLR of 21.52%. This is because each UE achieves the maximum MCS possible in the considered indoor conference scenario, owing to the full transmit power of the BS being assigned to the UE (compared to the MU-MIMO case where transmit power gets divided by the number of UEs co-scheduled) and complete absence of interference. Even though a second layer is allowed per UE, we hardly see the RI reported as two since the propagation environment itself is fewer rich, i.e. there's less multi-path, so there are less paths to take anyway and also, the additional layer (of the same UE) if reported, brings some interference. This behaviour is reflected in the same PLR performance for both $single-rank$ and $dual-rank$ cases.

4.1.3 Impact of Type I and Type II CSI on MU-MIMO technology

Understanding the impact of $Type\ I$ and $Type\ II$ CSI feedback methods on the system performance is a pivotal part of the thesis. As detailed in Chapter 2, the difference between the two methods is the use of a linear combination of two, three or four beams with significant power-scaling factors (for $L = 2,\ 3,\ 4$) in $Type\ II$, instead of a single beam in $Type\ I$. The impact of L was investigated for both the 'fixed-RF' and the 'adaptive-RF' cases, however, for the latter case we observed no benefit of $L > 1$ since under 'adaptive-RF', and given the assumed propagation environment, a UE's second-strongest is too weak to be worthwhile. For the 'fixed-RF' case we observe potentially a larger impact of L and therefore investigate this in more detail through the different charts.

Figure 4.4 shows the performance of the MU-MIMO setting of the conference scenario

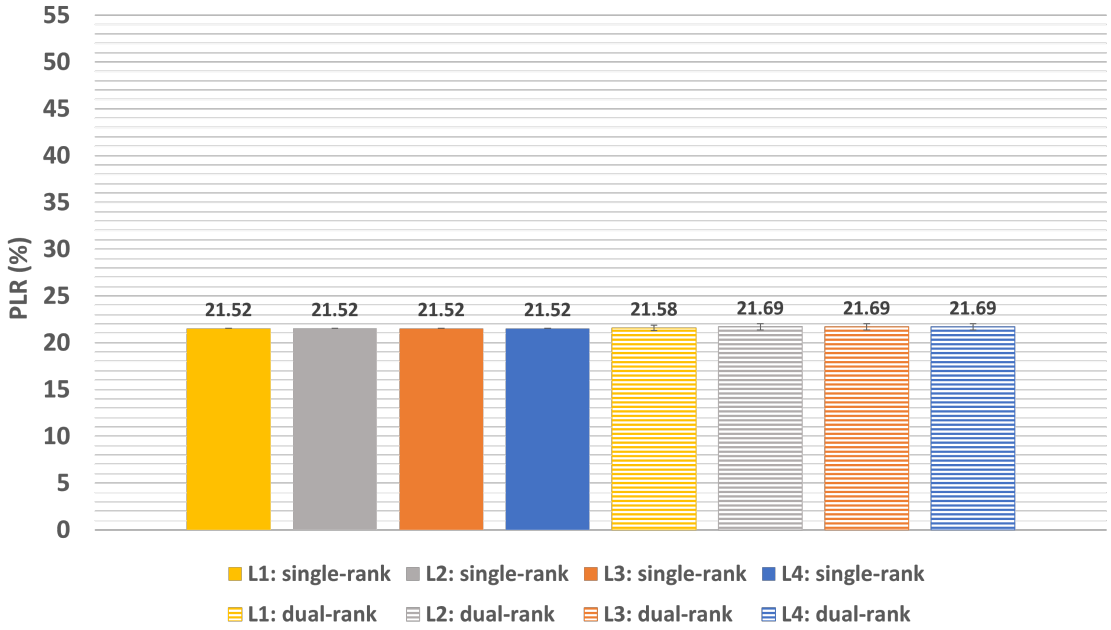

Figure 4.3: SU-MIMO average PLR across all UEs and simulated meetings for comparing the system performance when *Type I* and *Type II* CSI feedback techniques are used for different transmission ranks (Rank 1 and Rank 2) with a fixed-RF 3 for 3.5 GHz.

where *Type I* ($L = 1$) and *Type II* ($L = 2,\ 3,\ 4$) CSI methods are used for both *single* and $dual - rank$ cases. The mentioned combinations are simulated for different γ values of $\{0, 0.2, 0.4, 0.6, 0.8, 1\}$.

Impact of γ

When we set a bigger γ, on one hand we essentially increase the inter-layer interference threshold, allowing more UEs to be co-scheduled which generally leads to a lower SINR and gets translated to a lower MCS and throughput for the particular UEs involved in the interference thread. To compensate this, UEs with lower MCSs are served more often which has an increasing impact on the UEs' throughput. In our scenario, we observe that the net effect of the above trade-off is a PLR increase with an increase in γ value for both *Type I* and *Type II* $single - rank$ cases.

In the PLR trend of the $dual - rank$ case across the γ range, we can observe that the PLR decreases when the γ value increases from 0 to 0.2 and then further increases when the γ increases from 0.2 up till unity. In such cases, the γ value (0.2 in this case) to the either sides of which the PLR increases, marks the right balance between co-scheduling the apt number of users with least possible interference. At $\gamma = 0.2$, the co-scheduling of UEs improves significantly (compared to $\gamma = 0$) to overcome the interference encountered due to the increase of γ. This results in a lower PLR value at 0.2 compared to 0. However, further increase from 0.2 causes higher interference which overshadows the co-scheduling throughput improvement and hence the PLR increases. Therefore, any γ lower than 0.2 yields a higher PLR because users are scheduled less frequently. Unlike the $dual - rank$ case, for $single - rank$ case, we observe a steady increase in the PLR with γ which is attributed to the interference of the UEs within the γ range overpowering the effect of

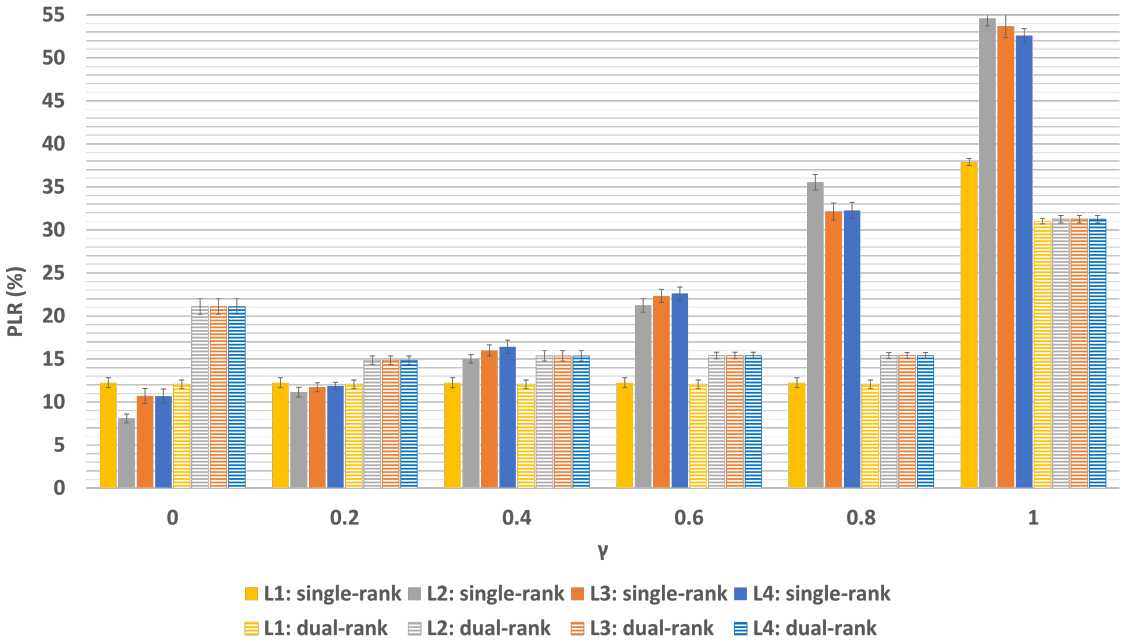

Figure 4.4: Average PLR across all UEs and simulated meetings for comparing the system performance when $Type\ I$ and $Type\ II$ CSI feedback techniques are used for different ranks ($single$ and $dual-rank$) with a fixed-RF 3 for 3.5 GHz. Different γ values {0, 0.2, 0.4, 0.6, 0.8, 1} are considered.

increase in throughput due to more frequent scheduling of the affected UEs.

Impact of Type I and Type II CSI feedback methods

In a MU-MIMO scenario, when the number of precoder beams used for the creation of the LC precoder increases ($L = 1$ for $Type\ I$ and $L = 2, 3, 4$ for $Type\ II$), we observe that the impact is different for different settings of γ and supported transmission ranks. This is due to the fact that, an increase in L for one UE can impact the interference effect it causes on the other co-scheduled UEs in different ways. For example, as illustrated in Figure 4.5, let's consider a case with three UEs co-scheduled with $L = 1$ (UE_1, UE_2, UE_3) where the precoder used by UE_1 creates heavy interference on UE_2 and does not impact UE_3. If L is increased to 2, suppose that the second precoder added to UE_1 creates no impact to UE_2 but some interference to UE_3. We then find that for $L = 2$ the selected LC precoder for UE_1 effectively reduces the interference towards UE_2 while it increases the interference towards UE_3. This example illustrates how indeed a change in configuration from L = 1 ($Type\ I$) to L = 2 ($Type\ II$) can have both a positive and a negative interference effect, supporting the observed absence of a clear trend in the bottom-line performance of L. For the considered case, we observe that $L = 1$ performs better than $L = 2,\ 3,\ 4$ for all $dual-rank$ case and $L = 2$ performs best for the $single-rank$ case. Thus the best choice of CSI feedback method for an indoor conference scenario with a similar setting is $Type\ II$ with $L = 2$ for $single-rank$ case and $Type\ I$ for $single-rank$ case.

Impact of different transmission ranks

For $Type\ I$ method, we observe that $dual-rank$ performs similar to $single-rank$ for γ values up to unity (PLR of 12.08%). For the γ value of unity, we can see that

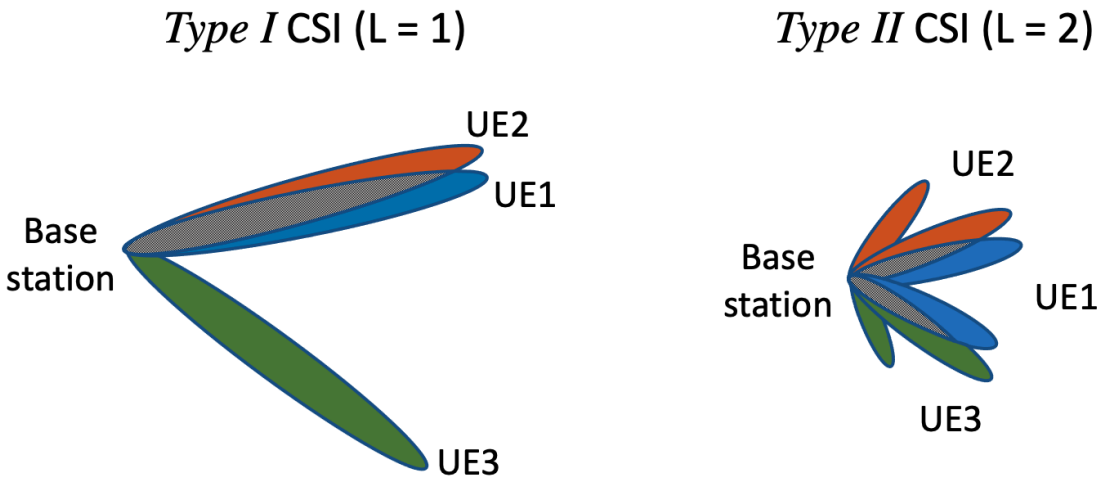

Figure 4.5: Example illustration depicting the interference dynamics for UEs when *Type I* and *Type II* ($L = 2$) CSI feedbacks are used.

the $dual - rank$ outperforms $single - rank$ with a PLR of 31% compared to the 37.89% recorded for the latter. This happens because of the fact that the γ value of unity allows for the co-scheduling of two UEs even if they select the exact same beam (which can happen very often considering the availability of only 16 beams available per 'fixed-RF' for the total of 16 UEs) causing heavy interference in $single - rank$ case. If there are two layers splitting the transmit power - which means a reduction in interference for the first layer - of these highly interfering beams, the non-interfering second layers for the corresponding UEs can still fetch some throughput.

For *Type II* CSI, we observe similar trend as *Type I* for the high γ values (values $>$ 0.2) in the sense that $dual - rank$ outperforms $single - rank$. For the lower γ values of 0 and 0.2, $single - rank$ outperforms $dual - rank$. For the low γ cases, the behaviour is because of the increased interference caused by the additional layers of the $dual - rank$ case (i.e. the second layer added to each UE for the $dual - rank$ case can cause interference to the layers of other UEs). For the high γ cases, as explained above, the behaviour is because of the reduced interference resulting from the throughput compensation due to an additional non-interfering layer in $dual - rank$ which also splits the power of the otherwise interfering single layer.

4.2 Performance analysis for 26 GHz

This section details the observations and analysis of the results pertaining to the 26 GHz frequency band. The performance comparison of the 'fixed-RF' and 'adaptive-RF' is elaborated in section 4.1.1. Sections 4.1.2 and 4.1.3 contain the performance analysis of SU-MIMO and MU-MIMO technologies when *Type* and *Type II* CSI feedback methods are used for different values of γ and transmission ranks. There are two major aspects distinguishing the insights of the 26 GHz frequency band from the 3.5 GHz band. Firstly, the beams generated from the 26 GHz frequency band antenna are narrower compared to that of its sub-6 GHz counterpart since the former contains more antenna elements (presented in Figure 3.2). While narrower beams has less possibility of mutual non-orthogonality, the impact of interference can be very high in case of non-orthogonal beams.

Secondly, the base codebook used by the 26 GHz frequency is completely different from that used by the 3.5 GHz band.

4.2.1 Fixed-RF and adaptive-RF

For 26 GHz, Figure 4.6 illustrates the performance of the considered Social XR scenario when all the UEs are served with single best beam ($L = 1$) from each of the 16 RFs and for the 'adaptive-RF' case with different γ values. Once again we can see that the 'adaptive-RF' outperforms the 'fixed-RF' case (least PLR as red bar marked at 27.32% for RF 12) where the lowest PLR values observed are 0.95% for γ values of 0.4 and 0.6. These are ideal for the video streaming application and are well below the 5% requirement. We can find that the optimal γ for 26 GHz frequency band is higher from that found for the 3.5 GHz band (0 and 0.2). This can be attributed to the different codebooks of the two frequency bands which results in different interference patterns among the co-scheduled UEs, and for the 26 GHz band and its associated codebook, the right balance between the interference and co-scheduling trade-off occurs at 0.4 and 0.6. The trade-off mentioned for the 'adaptive-RF' case in the 3.5 GHz frequency band applies to 26 GHz band as well (Section 4.1.1).

We can also observe that the PLRs for the 26 GHz frequency band are higher compared to those of the 3.5 GHz band. This is attributed to the extremely high interference of the narrow non-orthogonal beams used by the co-scheduled UEs and the difference in the base codebook used compared to the 3.5 GHz frequency band.

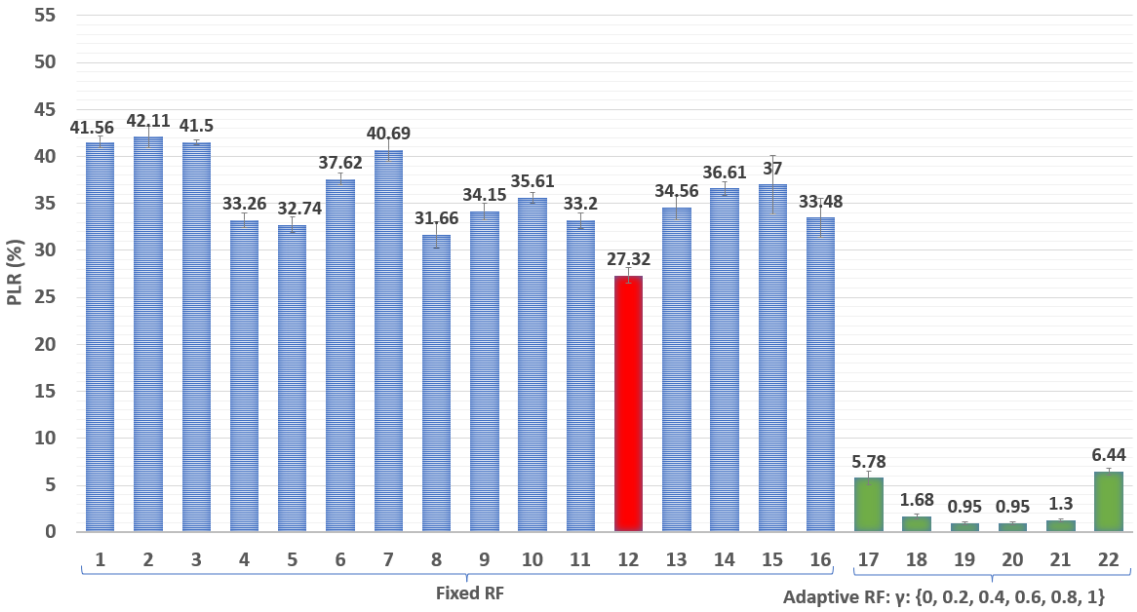

Figure 4.6: Average PLR across all UEs and simulated meetings for comparing the performance when fixed-RF and adaptive-RF are used for 26 GHz. The blue color-coded bars (and red bar representing the least PLR recorded among the 'fixed-RF' cases for RF 12) represent the PLR when all UEs select their precoders from a fixed-RF (1-16) and the green color-coded bars represent the PLR when the UEs use adaptive-RF and individually select the best RF for different γ values {0, 0.2, 0.4, 0.6, 0.8, 1}.

4.2.2 Impact of Type I and Type II CSI on SU-MIMO technology

Figure 4.7 shows the downlink performance for the XR environment when SU-MIMO technique is used for the 26 GHz frequency band. Since only single user is scheduled in a given TTI, a single-user scheduler does not have the γ parameter.

For the $single-rank$ case, we observe that each UE achieves the maximum MCS possible in the considered indoor conference scenario, owing to the full transmit power of the BS being assigned to the UE (compared to the MU-MIMO case where transmit power gets divided by the number of UEs co-scheduled) and complete absence of interference. The reason for the PLR of 27.57% despite of achieving highest MCS possible, is the reduced number of times each UE is scheduled (once every 16 TTIs). For the same reason, we see the same average PLR for both $Type\ I$ and $Type\ II$.

For the $dual-rank$ case, it is not always the highest MCS that is selected every TTI for each UE, since the transmit power per layer is half of the BS transmit power and also there is some inter-layer interference present in case the scheduler indeed decides to co-schedule multiple transmission layers. With the error bars taken into consideration, we observe that the $dual-rank$ PLR performance is similar for different L values and also matches the $single-rank$ PLR of 27.57%. This is because each UE achieves the maximum MCS possible in the considered indoor conference scenario, owing to the full transmit power of the BS being assigned to the UE (compared to the MU-MIMO case where transmit power gets divided by the number of UEs co-scheduled) and complete absence of interference. Even though a second layer is allowed per UE, we hardly see the RI reported as two since the propagation environment itself is less rich, i.e. there's less multi-path, so there are less paths to take anyway and also, the additional layer (of the same UE) if reported, brings some interference. This behaviour is reflected in the same PLR performance for both $single-rank$ and $dual-rank$ cases.

4.2.3 Impact of Type I and Type II CSI on MU-MIMO technology

Figure 4.8 shows the performance of the conference scenario where both $Type\ I$ ($L = 1$) and $Type\ II$ ($L = 2,\ 3,\ 4$) CSI methods are used for the $single$ and the $dual-rank$ cases. The mentioned combinations are simulated for different γ values of {0, 0.2, 0.4, 0.6, 0.8, 1}.

Impact of γ

In the 26 GHz frequency band, for $single-rank$ case, we observe a steady increase in the PLR with γ which is attributed to the interference of the UEs within the γ range overpowering the effect of increase in throughput due to more frequent scheduling of the affected UEs. For the $dual-rank$ case, we observe that any γ lower than 0.4 yields a higher PLR because users are scheduled less frequently and further increase from 0.6 causes higher interference which overshadows the co-scheduling throughput improvement and hence the PLR increases.

Impact of Type I and Type II CSI feedback methods

Like the 3.5 GHz frequency band, in the 26 GHz band MU-MIMO scenario, when the number of precoder beams used for the creation of the LC precoder increases ($L = 1$ for $Type\ I$ and $L = 2, 3, 4$ for $Type\ II$), we observe that the impact is different for different

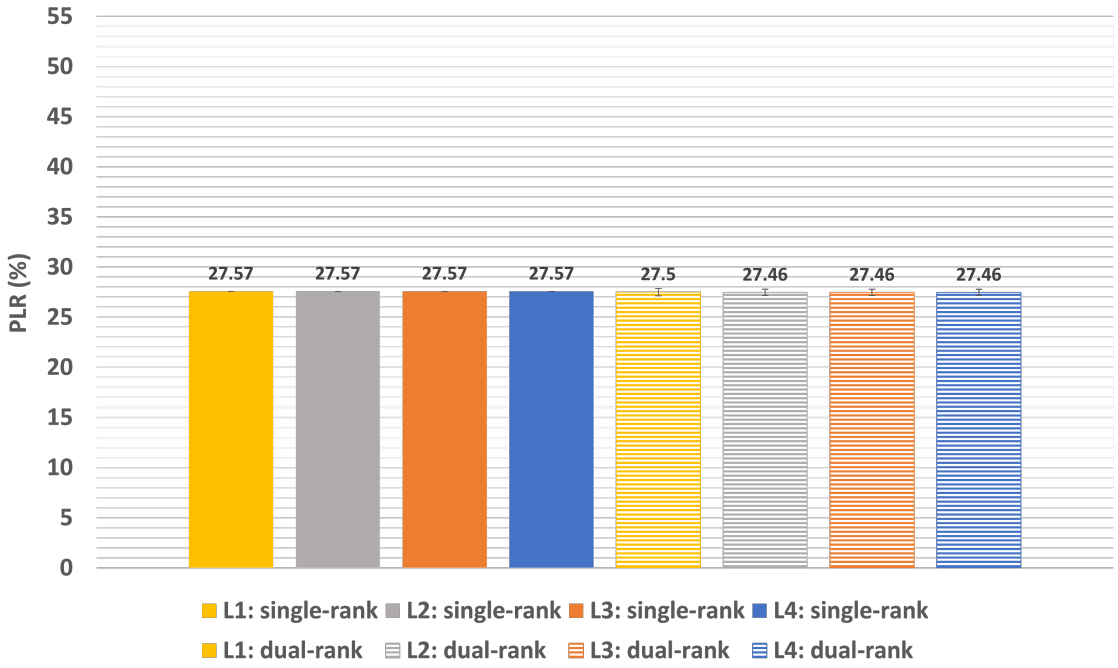

Figure 4.7: SU-MIMO average PLR across all UEs and simulated meetings for comparing the system performance when *Type I* and *Type II* CSI feedback techniques are used for different transmission ranks (Rank 1 and Rank 2) with a fixed-RF 12 for 26 GHz.

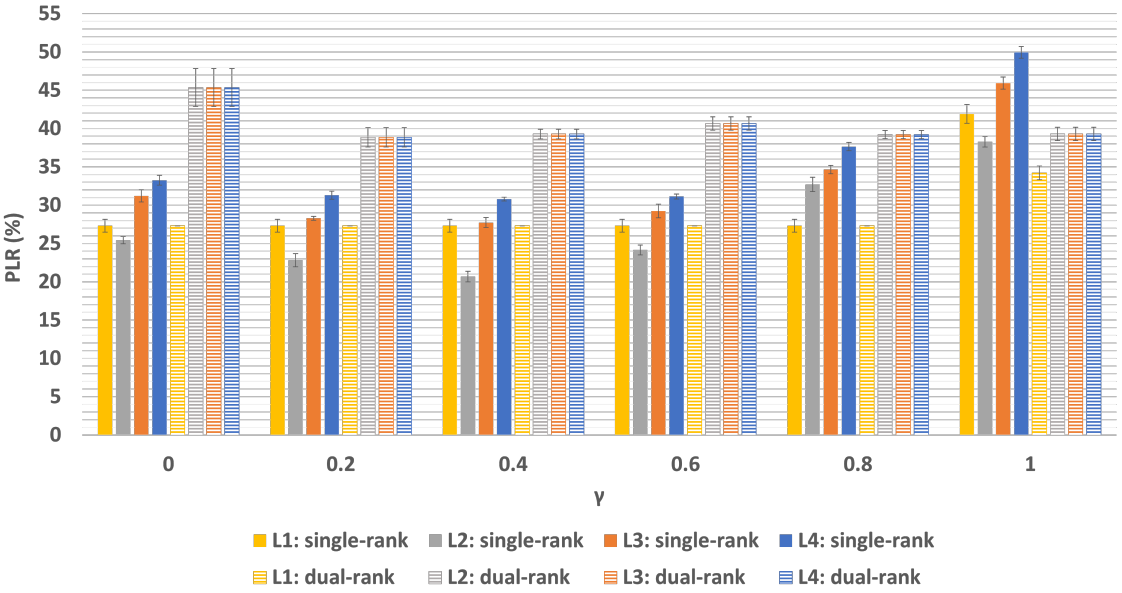

Figure 4.8: Average PLR across all UEs and simulated meetings for comparing the system performance when *Type I* and *Type II* CSI feedback techniques are used for different transmission ranks (*single* and $dual-rank$) with a fixed-RF 12 for 26 GHz. Different γ values $\{0, 0.2, 0.4, 0.6, 0.8, 1\}$ are used for plotting the PLR for aforementioned parameter combinations.

γ and transmission ranks (explanation of 3.5 GHz from Section 4.1.3 holds here). For the considered case, we observe that $L = 1$ performs better than $L = 2,\ 3,\ 4$ for all $dual-rank$

cases and $L = 2$ performs best for the $single - rank$ case. Thus the best choice of CSI feedback method for an indoor conference scenario with a similar setting is $Type\ II$ with $L = 2$ for $single - rank$ case and $Type\ I$ for $single - rank$ case.

Impact of different transmission ranks

For $Type\ I$ method, we observe that $dual - rank$ performs similar to $single - rank$ for γ values up to unity (PLR of 27.30%). For the γ value of unity, we can see that the $dual - rank$ outperforms $single - rank$ with a PLR of 34.21% compared to the 41.91% recorded for the latter. This happens because of the fact that the γ value of unity allows for the co-scheduling of two UEs even if they select the exact same beam (which can happen very often considering the availability of only 16 beams available per 'fixed-RF' for the total of 16 UEs) causing heavy interference in $single - rank$ case. If there are two layers splitting the transmit power - which means a reduction in interference for the first layer - of these highly interfering beams, the non-interfering second layers for the corresponding UEs can still fetch some throughput.

For $Type\ II$ CSI, we observe similar trend as $Type\ I$ for the high γ values (values $>$ 0.6) in the sense that $dual - rank$ outperforms $single - rank$. For the lower γ values, $single - rank$ outperforms $dual - rank$. For the low γ cases, the behaviour is because of the increased interference caused by the additional layers of the $dual - rank$ case (i.e. the second layer added to each UE for the $dual - rank$ case can cause interference to the layers of other UEs). For the high γ cases, as explained above, the behaviour is because of the reduced interference resulting from the throughput compensation due to an additional non-interfering layer in $dual - rank$ which also splits the power of the otherwise interfering single layer.

4.3 Bandwidth analysis for the ideal scenario

From the PLRs recorded in Figures 4.2, 4.4, 4.6 and 4.8, it is evident that for MU-MIMO, the use of adaptive-RFs with γ values of 0.2 for 3.5 GHz and 0.4 for 26 GHz suit our scenario the best. Triggered by the observation that the PLR is lower than needed, which suggests that a reduced carrier bandwidth may suffice, in this section, we try to analyse the impact of different bandwidths on these ideal cases. Figure 4.9 shows the PLR trend for the 'adaptive-RF' case for both the 3.5 GHz and 26 GHz frequency bands for four different bandwidth values of (100, 200, 300 and 400 MHz). With an admissible value of 5% PLR, we can see that even with a bandwidth smaller than the previously considered 400 MHz (200 MHz (and above) for the 3.5 GHz band and 300 MHz (and above) for the 26 GHz band), we can achieve tolerable downlink performance for the given Social XR scenario.

In addition to the ideal case above, we also try to understand the bandwidth requirement to achieve 5% PLR for the best observed 'fixed-RF' cases ($\gamma = 0$ and $L = 2$ for the 3.5 GHz frequency band and $\gamma = 0.4$ and $L = 2$ for the 26 GHz frequency band). Figure 4.10 shows the PLR trend for the 'fixed-RF' case for the 3.5 GHz frequency band with bandwidth values of (400, 500, 600 and 700 MHz) and the 26 GHz frequency band with bandwidth values of (900, 1100, 1200 and 1300 MHz). We can see that with a bandwidth of 600 MHz (and above) for the 3.5 GHz band and 1300 MHz (and above) for the 26 GHz band, we can achieve tolerable downlink performance for the given Social XR scenario.

We can also see that the bandwidth required by the 26 GHz frequency band is higher than that required by the 3.5 GHz band. There are two reasons for this observation. Firstly, as discussed in Section 4.2, the narrow beams of 26 GHz create very high interference when they are non-orthogonal and this causes high PLR compared to the wide beams of 3.5 GHz. Secondly, the cases compared here use a higher γ of 0.4 for 26 GHz compared to 0.2 for 3.5 GHz, which means more interference occurrence is permitted between the co-scheduled UEs.

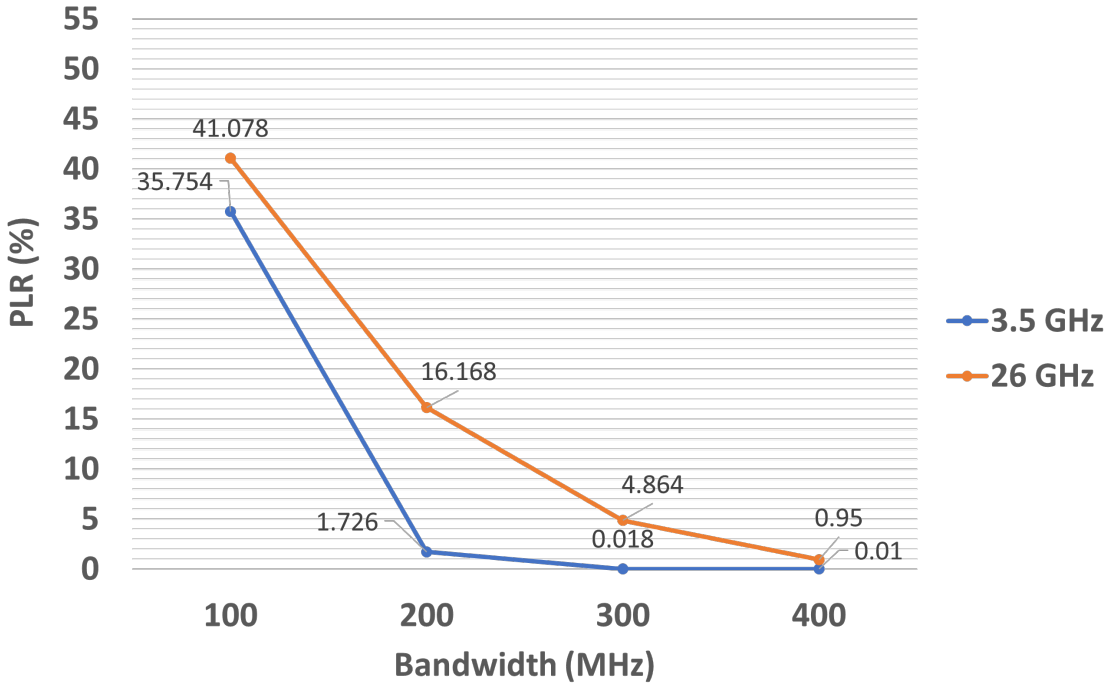

Figure 4.9: Average PLR across all UEs and simulated meetings for comparing the system performance when different bandwidths are used for the observed ideal 'adaptive-RF' case. γ values of 0.2 and 0.4 are used for the 3.5 GHz and the 26 GHz frequency bands, respectively.

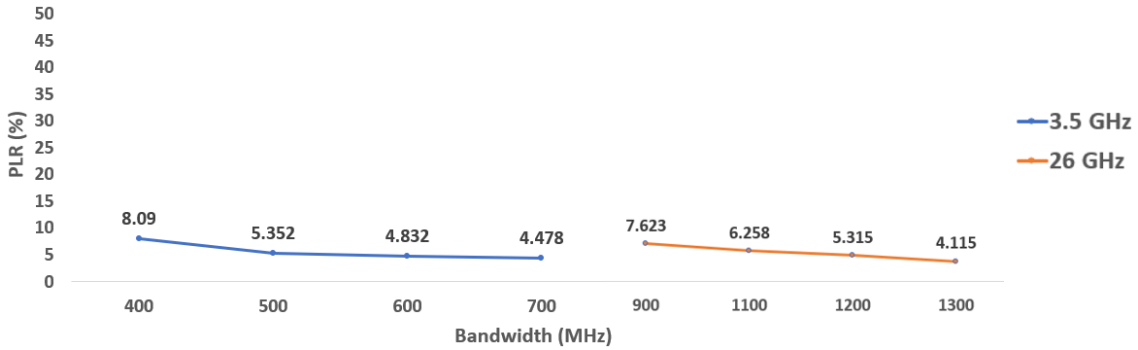

Figure 4.10: Average PLR across all UEs and simulated meetings for comparing the system performance when different bandwidths are used for the observed best 'fixed-RF' case. γ values of 0 and 0.4 are used for the 3.5 GHz and the 26 GHz frequency bands, respectively.

Chapter 5

Conclusion and future work

5.1 Conclusion

Social XR applications are throughput-intensive applications gaining immense popularity with the introduction of 5G. In this thesis we have presented a simulation-based performance assessment for an indoor Social XR conference scenario involving a fixed number of physical and virtual participants. More specifically, the thesis attempts to provide an insight in to how such an application's radio downlink performance is impacted when we consider different carrier frequency bands, CSI feedback methods, RFs, MIMO techniques, ranks and γ values using the key metric of PLR.

To this end, we have modeled and implemented all key scenario aspects, including the conference setting, the Social XR application, the indoor propagation environment, the 5G base station, its deployed massive MIMO antenna, the defined beamforming codebooks, the CSI feedback options, and the packet scheduling scheme. We understand how together with the different MIMO, CSI techniques and transmission ranks, the RF and γ also form important configurable parameters which can affect the system performance significantly.

Considering the main results, for each of the frequency bands of 3.5 GHz and 26 GHz, we have compared the use of 'fixed-RF' and 'adaptive-RF', the impact of $Type\ I$ and $Type\ II$ CSI on SU-MIMO and MU-MIMO under $single$ and $dual-rank$ scenarios. Finally we perform bandwidth analysis for the best configurations observed (i.e. the 'adaptive-RF' case with an optimised γ). The key findings from the analysis of the simulated results are as follows:

- For both frequency bands, the 'adaptive-RF' case substantially outperforms the 'fixed-RF' case, where the former yields significantly lower PLR values. This is owing to the fact that the UEs individually gets to pick the best beam or the LC beams in the 'adaptive-RF' case compared to the 'fixed-RF' case, where there is a restricted set of available beams depending on the assigned RF.
- For the considered conference setting, the PLRs for 26 GHz frequency band are found to be higher compared to those of the 3.5 GHz band. This is however noted to be entirely subjective to the positions of the UEs with respect to the beams selected by them and the interference encountered. The precoders and the angles spanned by them are completely different for the two frequency bands. Also, the 26 GHz frequency band is characterised by more narrower beams compared to the 3.5 GHz

band (even if the probability of non-orthogonality between beams is low for such narrow beams, the interference for the non-orthogonal beams are very high because of the higher gains).

- When configuring a relatively high γ for a MU-MIMO case, more UEs get co-scheduled, and also with a lower tx power, however with a potentially higher interference (hence lower SINR and hence lower MCS) which may lead to higher PLR, if the resulting low throughput is not compensated for by the more frequent scheduling of the UEs. For the 3.5 GHz 'adaptive-RF' case, we observe that this compensation is not enough for any value of γ and that the PLR increases with the γ. For 26 GHz 'adaptive-RF' case, the compensation works from $\gamma = 0$ to $\gamma = 0.4$, where the PLR reduces, but further fails from 0.4 to unity, causing the PLR to increase. We find similar trends in the 'fixed-RF' MU-MIMO cases as well for both frequency bands, CSI Types and ranks.

- For for both frequency bands and assuming the 'adaptive-RF' setting in MU-MIMO scenarios, we observe the same performance for the different CSI feedback methods and allowable transmission ranks. This is because, under 'adaptive-RF', and given the assumed propagation environment, a UE's second-strongest is too weak to be worthwhile.

- In MU-MIMO scenarios with the 'fixed-RF' setting, we observe different PLR trends for $Type\ I$ ($L = 1$) and $Type\ II$ (L= 2, 3, 4) CSI feedback methods while using different frequency bands, γ and transmission ranks. This is due to the additional ($L > 1$) beams of the co-scheduled UEs impacting each other differently, causing simultaneous increase in interference for some UEs and decrease in interference for others, thereby producing different net effects for different frequency bands, γ and transmission ranks. For both frequency bands, the optimal choice of CSI feedback method for the presented scenarios with a similar setting is $Type\ II$ with $L = 2$ for $single - rank$ case and $Type\ I$ for $single - rank$ case.

- In MU-MIMO scenarios with the 'fixed-RF' setting, the $dual-rank$ case outperforms $single - rank$ for higher values of γ and gives lower (for $Type\ II$ CSI) or equal performance (for $Type\ I$ CSI) for lower values of γ. For the low γ cases, the behaviour is because of the increased interference caused by the additional layers of the $dual - rank$ case (i.e. the second layer added to each UE for the $dual - rank$ case can cause interference to the layers of other UEs). For the high γ cases, the behaviour is because of the reduced interference resulting from the throughput compensation due to an additional non-interfering layer in $dual - rank$ which also splits the power of the otherwise interfering single layer.

- In SU-MIMO scenarios with the 'fixed-RF' setting for both frequency bands, the PLR performance is similar for different L values and ranks. This is because each UE achieves the maximum MCS possible in the considered indoor conference scenario, owing to the full transmit power of the BS being assigned to the UE (compared to the MU-MIMO case where transmit power gets divided by the number of UEs co-scheduled) and complete absence of interference. Even though a second layer is allowed per UE, we hardly see the RI reported as two since the propagation environment itself is less rich, i.e. there's less multi-path, so there are less paths to take anyway and also, the additional layer (of the same UE) if reported, brings some interference. This behaviour is reflected in the same PLR performance for both $single - rank$ and $dual - rank$ cases.

- Finally, for the overall best performance found in the 'adaptive-RF' case, we observe that for the frequency band of 3.5 GHz, any bandwidth of 200 MHz or above would suffice for achieving the target PLR of 5%. For the 26 GHz band, any bandwidth greater than or equal to 300 MHz will suffice for the target PLR. For the overall best performance found in the 'fixed-RF' case, we observe that for the frequency band of 3.5 GHz, any bandwidth of 600 MHz or above would suffice for achieving 5% PLR. For the 26 GHz band, any bandwidth greater than or equal to 1300 MHz will suffice. We can observe that the minimum bandwidth required for 26 GHz frequency band is higher compared to the 3.5 GHz band for both the 'fixed-RF' and the 'adaptive-RF' cases and this occurs because of the reason stated in the second bullet.

- Overall, for the considered Social XR conference scenario, we conclude that the best performance configurations include the use of 'adaptive-RF' with γ values of 0 or 0.2 for the 3.5 GHz frequency band and 0.4 or 0.6 for the 26 GHz frequency band and that this performance holds for both $Type\ I$ and $Type\ II$ CSI feedback methods as well for the $single-rank$ and $dual-rank$ cases.

5.2 Future work

The following enlisted ideas are identified as potential future scope areas which can significantly contribute to further enriching the work presented through this thesis.

- Considering the compatibility of SRS-based CSI feedback methods for TDD systems, a good future scope will be an exclusive comparison study of the SRS-based method (for the short distance considered between the BS and UE, SRS-based method is expected to give good performance) with the already implemented codebook-based CSI feedback method.

- Since the present work is restricted to an indoor scenario, to further validate the obtained insights, an outdoor environment setting can be considered and the downlink performance can be analysed. Further, Non Line of Sight (NLOS) scenario can be taken into account if UEs are spaced more than 50 m away from the BS in a realistic outdoor scenario and this can create a different impact due to the prominent multi-path components. The multi-path richness of the NLOS scenario increases the MIMO capacity, since it provides large number of eigenvalues of MIMO channel due to the presence of rich scatterers.

- Further with respect to the environment, user mobility can be expanded beyond the head movements since this will result in frequent change of precoders selected by the UEs. It will be an interesting study to analyse the adaptive-RF use case in such an environment, since heavy mobility cases require frequent update of precoders and this can cause high control signalling overhead for an adaptive-RF. Also, it will be worthwhile to compare the fixed- and adaptive-RF cases for either the same level of overhead or the same CSI periodicity, but then explicitly incorporating the higher overhead and the performance impact thereof in the modelling.

- 3GPP specific blockage models could be interwoven into the scenario to further and realistically extend the diversity of the possible propagation environments. For example, it is highly probable for a human blockage to occur when a participant walks into the meeting room or leaves the room.

- The interference estimation mechanism can be implemented using machine learning, where the present mechanism of book-keeping interference can contribute to creating the learning data set. Using these data sets, the performance of the downlink can be improved. ML-based interference estimations can be particularly relevant in case of multi-cell scenarios with inter-cell interference.

Bibliography

[1] 3GPP. *5G ;NR; Physical layer procedures for data*. TS 38.214. Version 16.2.0. July 2020.

[2] 3GPP. *Extended Reality (XR) in 5G*. TR 26.928. Version 16.0.0. 2020.

[3] 3GPP. *Home Node B (HNB) Radio Frequency (RF) requirements (FDD)*. TR 25.967. Version 16.0.0. 2020.

[4] 3GPP. *NR; User Equipment (UE) radio access capabilities*. TS 38.306. Version 16.4.0. 2021.

[5] 3GPP. *Technical specification group radio access network; study on channel model for frequencies from 0.5 to 100 GHz*. TR 38.901. Version 16.1.0. 2020.

[6] 3GPP. *WF on type I and II CSI codebook*. TS 38.214. Version 15.4.0. Dec. 2018. URL: https://portal.3gpp.org/Specifications.aspx?q=1&releases=190%20[3]%20Samsung%20etc.

[7] F. Adeyemi-Ejeye, M. Alreshoodi, L. Al-Jobouri, M. Fleury, and J. Woods. "Packet loss visibility across SD, HD, 3D, and UHD video streams". In: *Journal of Visual Communication and Image Representation* 45 (May 2017), pp. 95–106. DOI: 10.1016/j.jvcir.2017.02.012.

[8] F. Afroz, K. Sandrasegaran, and P. Ghosal. "Performance analysis of PF, M-LWDF and EXP/PF packet scheduling algorithms in 3GPP LTE downlink". In: *2014 Australasian Telecommunication Networks and Applications Conference (ATNAC)*. 2014, pp. 87–92. DOI: 10.1109/ATNAC.2014.7020879.

[9] E. Bastug, M. Bennis, M. Medard, and M. Debbah. "Toward interconnected virtual reality: opportunities, challenges, and enablers". In: *IEEE Communications Magazine* 55.6 (2017), pp. 110–117. DOI: 10.1109/MCOM.2017.1601089.

[10] K. Bechta, C. Ziółkowski, J. Kelner, and L. Nowosielski. "Modeling of downlink interference in massive MIMO 5G macro-cell". In: *Sensors* 21 (Jan. 2021), p. 597. DOI: 10.3390/s21020597.

[11] F. Burkhardt, S. Jaeckel, E. Eberlein, and R. Prieto-Cerdeira. "QuaDRiGa: A MIMO channel model for land mobile satellite". In: *The 8th European Conference on Antennas and Propagation (EuCAP 2014)*. 2014, pp. 1274–1278. DOI: 10.1109/EuCAP.2014.6902008.

[12] P. Butovitsch, D. Astely, T. Chapman, M. Frenne, F. Ghasemzadeh, M. Hagström, B. Hogan, G. Jöngren, J. Karlsson, F. Kronestedt, E. Larsson, and H. Asplund. *Advanced antenna systems for 5G network deployments - bridging the gap between theory and practice*. June 2020. ISBN: 9780128200469.

[13] E. David, J. Gutiérrez, A. Coutrot, M. Perreira Da Silva, and P. Le Callet. "A dataset of head and eye movements for 360° videos". In: June 2018, pp. 432–437. DOI: 10.1145/3204949.3208139.

[14] Z. Du. "Cross-layer Optimization of MAC Scheduling for Multi-User Virtual Reality over 5G". 2022.

[15] M. S. Elbamby, C. Perfecto, M. Bennis, and K. Doppler. "Toward low-latency and ultra-reliable virtual reality". In: *IEEE Network* 32.2 (2018), pp. 78–84. DOI: 10.1109/MNET.2018.1700268.

[16] S. Fremerey, A. Singla, K. Meseberg, and A. Raake. "AVtrack360: an open dataset and software recording people's head rotations watching 360° videos on an HMD". In: June 2018, pp. 403–408. DOI: 10.1145/3204949.3208134.

[17] A. Ghosh, R. Ratasuk, B. Mondal, N. Mangalvedhe, and T. Thomas. "LTE-advanced: next-generation wireless broadband technology [Invited Paper]". In: *IEEE Wireless Communications* 17.3 (2010), pp. 10–22. DOI: 10.1109/MWC.2010.5490974.

[18] B. Groß, R. A. Salem, T. Wild, and G. Wunder. *Explicit CSI feedback compression via learned approximate message passing*. 2021. arXiv: 2110.05837 [eess.SP].

[19] J. Hoydis, S. Ten Brink, and M. Debbah. "Massive MIMO in the UL/DL of cellular networks: How many antennas do we need?" In: *IEEE Journal on Selected Areas in Communications* 31.2 (2013), pp. 160–171. DOI: 10.1109/JSAC.2013.130205.

[20] H. Huh, G. Caire, H. C. Papadopoulos, and S. A. Ramprashad. "Achieving massive MIMO spectral efficiency with a not-so-large number of antennas". In: *IEEE Transactions on Wireless Communications* 11.9 (2012), pp. 3226–3239. DOI: 10.1109/TWC.2012.070912.111383.

[21] S. Kizhakkekundil, J. Morais, S. Braam, and R. Litjens. "Four knife-edge diffraction with antenna gain model for generic blockage modelling". In: *IEEE Wireless Communications Letters* 10.10 (2021), pp. 2106–2109. DOI: 10.1109/LWC.2021.3093197.

[22] Y. Liao, H. Yao, Y. Hua, and C. Li. "CSI feedback based on deep learning for massive MIMO systems". In: *IEEE Access* 7 (2019), pp. 86810–86820. DOI: 10.1109/ACCESS.2019.2924673.

[23] D. J. Love and R. W. Heath. "Equal gain transmission in multiple-input multiple-output wireless systems". In: *IEEE Transactions on Communications* 51.7 (2003), pp. 1102–1110. DOI: 10.1109/TCOMM.2003.814195.

[24] D. J. Love and R.W. Heath. "Limited feedback unitary precoding for spatial multiplexing systems". In: *IEEE Transactions on Information Theory* 51.8 (2005), pp. 2967–2976. DOI: 10.1109/TIT.2005.850152.

[25] D. J. Love, R.W. Heath, and T. Strohmer. "Grassmannian beamforming for multiple-input multiple-output wireless systems". In: *IEEE Transactions on Information Theory* 49.10 (2003), pp. 2735–2747. DOI: 10.1109/TIT.2003.817466.

[26] S. Mangiante, G. Klas, A. Navon, G. Zhuang, J. Ran, and M. Silva. "VR is on the edge: How to deliver 360° videos in mobile networks". In: Aug. 2017, pp. 30–35. DOI: 10.1145/3097895.3097901.

[27] T. L. Marzetta. "Non-cooperative cellular wireless with unlimited numbers of base station antennas". In: *IEEE Transactions on Wireless Communications* 9.11 (2010), pp. 3590–3600. DOI: 10.1109/TWC.2010.092810.091092.

[28] H. Miao, M. D. Mueck, and M. Faerber. "Amplitude quantization for Type-2 codebook based CSI feedback in New Radio system". In: *2018 European Conference on Networks and Communications (EuCNC)*. 2018, pp. 1–9. DOI: 10.1109/EuCNC.2018.8442609.

[29] J. Morais. "Performance Modelling for Social VR Conference Applications in Beyond-5G Radio Access Networks,"" Feb 2021.

[30] J. Morais, S. Braam, R. Litjens, S. Kizhakkekundil, and J. L. van den Berg. "Performance modelling and assessment for Social VR conference applications in 5G radio networks". In: 17th International Conference on Wireless and Mobile Computing, Networking and Communications, WiMob '21 ; Conference date: 11-10-2021 Through 13-10-2021. 2021. URL: http://www.wimob.org/wimob2021/.

[31] C. Muhan, G. Jiajia, C. Wen, S. Jin, G. Li, and A. Yang. *Deep Learning-based implicit CSI feedback in massive MIMO*. May 2021.

[32] M. Müller, F. Ademaj, T. Dittrich, A. Fastenbauer, B. Elbal, A. Nabavi, L. Nagel, S. Schwarz, and M. Rupp. "Flexible multi-node simulation of cellular mobile communications: the Vienna 5G system level simulator". In: *EURASIP Journal on Wireless Communications and Networking* 2018 (Sept. 2018). DOI: 10.1186/s13638-018-1238-7.

[33] S. Pratschner, B. Tahir, L. Marijanovic, M. Mussbah, K. Kirev, R. Nissel, S. Schwarz, and M. Rupp. "Versatile mobile communications simulation: the Vienna 5G Link Level Simulator". In: *EURASIP Journal on Wireless Communications and Networking* 2018 (Sept. 2018). DOI: 10.1186/s13638-018-1239-6.

[34] V. Raghavan, R. W. Heath, and A. M. Sayeed. "Systematic codebook designs for quantized beamforming in correlated MIMO channels". In: *IEEE Journal on Selected Areas in Communications* 25.7 (2007), pp. 1298–1310. DOI: 10.1109/JSAC.2007.070804.

[35] F. Rusek, D. Persson, B. K. Lau, E. G. Larsson, T. L. Marzetta, O. Edfors, and F. Tufvesson. "Scaling up MIMO: opportunities and challenges with very large arrays". In: *IEEE Signal Processing Magazine* 30.1 (2013), pp. 40–60. DOI: 10.1109/MSP.2011.2178495.

[36] Samsung. *Massive MIMO for New Radio*. Tech. rep. Samsung, Dec. 2020.

[37] S. Sun, G. Maccartney, and T.S. Rappaport. "A novel millimeter-wave channel simulator and applications for 5G wireless communications". In: May 2017, pp. 1–7. DOI: 10.1109/ICC.2017.7996792.

[38] H. Tataria, P. J. Smith, L. J. Greenstein, and P. A. Dmochowski. "Zero-forcing precoding performance in multiuser MIMO systems with heterogeneous Ricean fading". In: *IEEE Wireless Communications Letters* 6.1 (2017), pp. 74–77. DOI: 10.1109/LWC.2016.2631602.

[39] L. Wu, J. Chen, H. Yang, and D. Lu. "Codebook design for LTE-A downlink system". In: *2011 IEEE Vehicular Technology Conference (VTC Fall)*. 2011, pp. 1–5. DOI: 10.1109/VETECF.2011.6092993.

[40] D. Yang, L.-L. Yang, and L. Hanzo. "DFT-based beamforming weight-vector codebook design for spatially correlated channels in the unitary precoding aided multiuser downlink". In: *2010 IEEE International Conference on Communications*. 2010, pp. 1–5. DOI: 10.1109/ICC.2010.5502350.

[41] ZTE. *5G Massive MIMO Network Application*. Tech. rep. ZTE, Sept. 2020.

Appendix A

RF and the associated precoder columns for $N_1 = N_2 = 8$.

Table A.1 shows the RFs 1 to 16 and the associated precoder columns for $N_1 = N_2 = 8$.

R1	R2	R3	R4	R5	R6	R7	R8	R9	R10	R11	R12	R13	R14	R15	R16
1	2	3	4	33	34	35	36	65	66	67	68	97	98	99	100
5	6	7	8	37	38	39	40	69	70	71	72	101	102	103	104
9	10	11	12	41	42	43	44	73	74	75	76	105	106	107	108
13	14	15	16	45	46	47	48	77	78	79	80	109	110	111	112
17	18	19	20	49	50	51	52	81	82	83	84	113	114	115	116
21	22	23	24	53	54	55	56	85	86	87	88	117	118	119	120
25	26	27	28	57	58	59	60	89	90	91	92	121	122	123	124
29	30	31	32	61	62	63	64	93	94	95	96	125	126	127	128
129	130	131	132	161	162	163	164	193	194	195	196	225	226	227	228
133	134	135	136	165	166	167	168	197	198	199	200	229	230	231	232
137	138	139	140	169	170	171	172	201	202	203	204	233	234	235	236
141	142	143	144	173	174	175	176	205	206	207	208	237	238	239	240
145	146	147	148	177	178	179	180	209	210	211	212	241	242	243	244
149	150	151	152	181	182	183	184	213	214	215	216	245	246	247	248
153	154	155	156	185	186	187	188	217	218	219	220	249	250	251	252
157	158	159	160	189	190	191	192	221	222	223	224	253	254	255	256
257	258	259	260	289	290	291	292	321	322	323	324	353	354	355	356
261	262	263	264	293	294	295	296	325	326	327	328	357	358	359	360
265	266	267	268	297	298	299	300	329	330	331	332	361	362	363	364
269	270	271	272	301	302	303	304	333	334	335	336	365	366	367	368
273	274	275	276	305	306	307	308	337	338	339	340	369	370	371	372
277	278	279	280	309	310	311	312	341	342	343	344	373	374	375	376
281	282	283	284	313	314	315	316	345	346	347	348	377	378	379	380
285	286	287	288	317	318	319	320	349	350	351	352	381	382	383	384
385	386	387	388	417	418	419	420	449	450	451	452	481	482	483	484
389	390	391	392	421	422	423	424	453	454	455	456	485	486	487	488
393	394	395	396	425	426	427	428	457	458	459	460	489	490	491	492
397	398	399	400	429	430	431	432	461	462	463	464	493	494	495	496
401	402	403	404	433	434	435	436	465	466	467	468	497	498	499	500
405	406	407	408	437	438	439	440	469	470	471	472	501	502	503	504
409	410	411	412	441	442	443	444	473	474	475	476	505	506	507	508
413	414	415	416	445	446	447	448	477	478	479	480	509	510	511	512
513	514	515	516	545	546	547	548	577	578	579	580	609	610	611	612
517	518	519	520	549	550	551	552	581	582	583	584	613	614	615	616
521	522	523	524	553	554	555	556	585	586	587	588	617	618	619	620
525	526	527	528	557	558	559	560	589	590	591	592	621	622	623	624
529	530	531	532	561	562	563	564	593	594	595	596	625	626	627	628
533	534	535	536	565	566	567	568	597	598	599	600	629	630	631	632
537	538	539	540	569	570	571	572	601	602	603	604	633	634	635	636
541	542	543	544	573	574	575	576	605	606	607	608	637	638	639	640
641	642	643	644	673	674	675	676	705	706	707	708	737	738	739	740
645	646	647	648	677	678	679	680	709	710	711	712	741	742	743	744
649	650	651	652	681	682	683	684	713	714	715	716	745	746	747	748
653	654	655	656	685	686	687	688	717	718	719	720	749	750	751	752
657	658	659	660	689	690	691	692	721	722	723	724	753	754	755	756
661	662	663	664	693	694	695	696	725	726	727	728	757	758	759	760
665	666	667	668	697	698	699	700	729	730	731	732	761	762	763	764
669	670	671	672	701	702	703	704	733	734	735	736	765	766	767	768
769	770	771	772	801	802	803	804	833	834	835	836	865	866	867	868
773	774	775	776	805	806	807	808	837	838	839	840	869	870	871	872
777	778	779	780	809	810	811	812	841	842	843	844	873	874	875	876
781	782	783	784	813	814	815	816	845	846	847	848	877	878	879	880
785	786	787	788	817	818	819	820	849	850	851	852	881	882	883	884
789	790	791	792	821	822	823	824	853	854	855	856	885	886	887	888
793	794	795	796	825	826	827	828	857	858	859	860	889	890	891	892
797	798	799	800	829	830	831	832	861	862	863	864	893	894	895	896
897	898	899	900	929	930	931	932	961	962	963	964	993	994	995	996
901	902	903	904	933	934	935	936	965	966	967	968	997	998	999	1000
905	906	907	908	937	938	939	940	969	970	971	972	1001	1002	1003	1004
909	910	911	912	941	942	943	944	973	974	975	976	1005	1006	1007	1008
913	914	915	916	945	946	947	948	977	978	979	980	1009	1010	1011	1012
917	918	919	920	949	950	951	952	981	982	983	984	1013	1014	1015	1016
921	922	923	924	953	954	955	956	985	986	987	988	1017	1018	1019	1020
925	926	927	928	957	958	959	960	989	990	991	992	1021	1022	1023	1024

Rotation factor
Precoder column in codebook matrix.

Figure A.1: RF and the associated precoder columns from the codebook matrix for $N_1 = N_2 = 8$.

Appendix B

BLER curves

Figure B.1 shows the BLER curves for the different MCS, with a 10% BLER probability marked for each curve. The curves are fitted to simulations based on the equations for each MCS curve that can be found in [29].

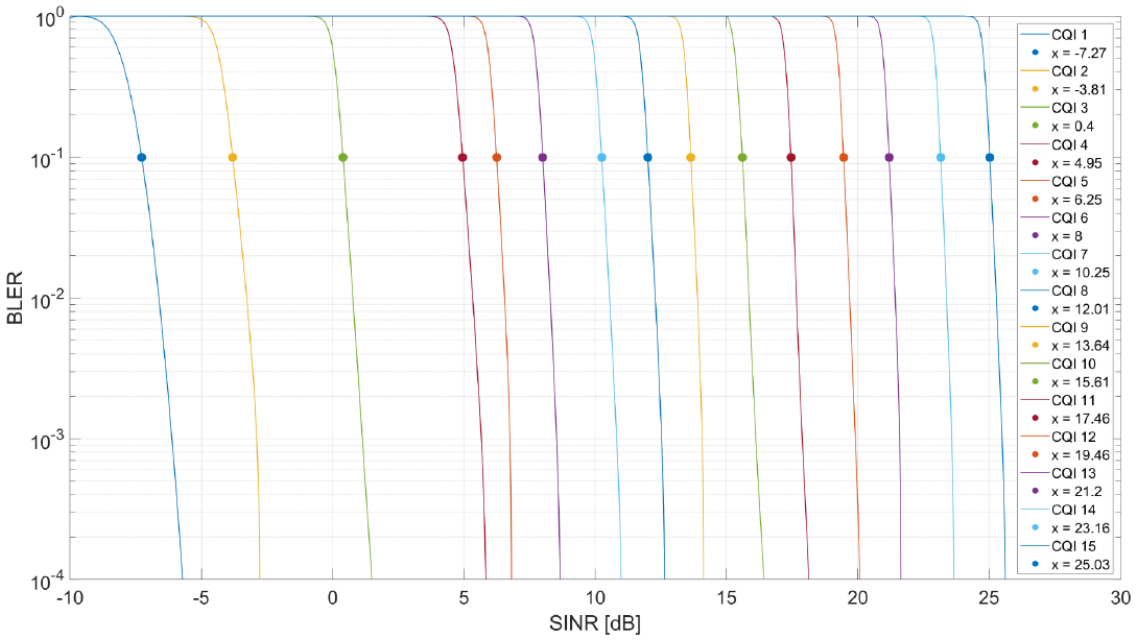

Figure B.1: BLER curves simulated with TU Vienna Link-Level Simulator [33].